Advances in single particle mass analysis

Szu-hsueh Lai, Sylvain Maclot, Rodolphe Antoine, Christophe D Masselon

Advances in Single Particle Mass Analysis.

Szu-Hsueh Lai* [1]; Sylvain Maclot[2] ; Rodolphe Antoine[2] and Christophe D. Masselon* [3,4,5]

[1] Department of Chemistry, National Cheng Kung University, Tainan TW-701, Taiwan.

[2] Institut Lumière Matière UMR 5306, Univ Lyon, Université Claude Bernard Lyon 1, CNRS, F-69100 Villeurbanne, France. rodolphe.antoine@univ-lyon1.fr

[3] CEA, IRIG, Laboratoire Biosciences et bioingénérie pour la Santé (EDyP team), F-38054 Grenoble, France.

[4] Inserm, Unité UA13, F-38054 Grenoble, France.

[5] Université Grenoble Alpes, F-38000 Grenoble, France.

* Corresponding authors: shlai@gs.ncku.edu.tw, christophe.masselon@cea.fr

Author Contributions

Szu-Hsueh Lai: formal analysis, investigation, writing–original draft, writing–review and editing. **Sylvain Maclot**: formal analysis, investigation, writing–review and editing. **Rodolphe Antoine**: conceptualization, writing–review and editing. **Christophe Masselon**: conceptualization, formal analysis, funding acquisition, project administration, resources, writing–original draft, writing–review and editing.

Acknowledgments

The authors gratefully acknowledge Mr. Po-Yu Chou from the Department of Chemistry at NCKU for his assisting with editing, Dr. Y. Tsybin from Spectroswiss Sàrl for providing the simulated time domain signals in Figure 3, as well as Drs M. Sansa and W. Trzpil from CEA LETI for helpful discussions on NEMS-MS and Figure 5. This work was supported in part by Taiwan's National Science and Technology Council (NSTC) funded project PAVISE (111-2628-M-006-007, 112-2628-M-006-010) and the program for Pandemic Prevention Science (112-2321-B-006-008, 113-2321-B-006-007), the Cross-Disciplinary Program on Instrumentation and Detection of CEA, the French Alternative Energies and Atomic Energy

Commission (project VIA-NEMS), as well as the French National Research Agency through projects AERONEMS (ANR-21-CE42-0028-01) and ProFI (ANR-10-INBS-08). R.A. acknowledges Agence Nationale de la Recherche (projects MANBAMM, ANR-21-CE29-0020, nanoGOLD, ANR-22-CE29-0022 and MOONSTONE, ANR-22-CE42-0031), the European Horizon 2020 research and innovation program's projects #964553 (ARIADNE) and HORIZON-EIC-2022-PATHFINDEROPEN-01 #101099058 (Virusong) for support.

Abstract

Single particle mass analysis methods allow the measurement and characterization of individual nanoparticles, viral particles, as well as biomolecules like protein aggregates and complexes. Several key benefits are associated with the ability to analyze individual particles rather than bulk samples, such as high sensitivity and low detection limits, and virtually unlimited dynamic range, as this figure of merit strictly depends on analysis time. However, data processing and interpretation of single particle data can be complex, often requiring advanced algorithms and machine learning approaches. In addition, particle ionization, transfer, and detection efficiency can be limiting factors for certain types of analytes. Ongoing developments in the field aim to address these challenges and expand the capabilities of single particle mass analysis techniques. Charge detection mass spectrometry is a single particle version of mass spectrometry in which the charge (z) is determine independently from *m/z*. Nano-electromechanical resonator mass analysis relies on changes in a nanoscale device's resonance frequency upon deposition of a particle to directly derive its inertial mass. Mass photometry uses interferometric video-microscopy to derive particle mass from the intensity of the scattered light. A common feature of these approaches is the acquisition of single particle data, which can be filtered and concatenated in the form of a particle mass distribution. In the present article, dedicated to our honored colleague Richard Cole, we cover the latest technological advances and applications of these single particle mass analysis approaches.

Keywords: Single particle mass spectrometry, Charge detection mass spectrometry, Nanoresonator mass spectrometry, Mass photometry.

Introduction

Mass Spectrometry (MS) originated from the field of physics at the beginning of the 20th century, and found initial applications in the separation of isotopes.[1] Over the years, its realm gradually expanded into chemistry, for the structural assessment of small organic molecules[2], then biochemistry to analyze larger biomolecules[3], and eventually biology with the characterization of gigantic supramolecular complexes[4]. As the field continued expanding its scope toward higher mass, MS encounters new challenges and converges with alternative technologies for mass measurement that are applicable in this upper mass range.

MS reliance on charge as a handle to gain access to the parameter of interest (i.e. mass) entails growing challenges as mass increases. In fact, large ions, particularly those generated by electrospray, carry many charges, which results in a multiplicity of species having closer and closer m/z ratios as the number of charges increases. Moreover, heterogeneities associated with chemical modifications, salt and solvent adducts, or simply from the sample itself containing variant species, further blur the picture, yielding intractable spectra in which charge state assignment becomes extremely challenging or even impossible.

One solution to this problem is to concurrently determine individual ions' charge (z) and mass to charge (m/z), building a mass distribution one particle at a time in an approach termed charge detection mass spectrometry (CDMS). As we will see in the following section, thanks to impressive progress over the past decade, CDMS became the leading technology for single particle mass analysis.[5] Adaptation of the CDMS method on widely used instrument platforms[6] and the anticipated release of dedicated commercial instruments bear witness to the vitality of the discipline[7].

Alternative solutions that diverge significantly from conventional MS methodologies use nano-mechanical or optical approaches to derive the particle's mass using vibrations or light scattering respectively.

Nano-Electro-Mechanical Sensor-based MS (NEMS-MS) directly determines the inertial mass of particles landing onto a vibrating nanostructure through changes in the structure's resonance frequency.[8] Like CDMS, NEMS-MS requires particle transfer into the gas phase, but its insensitivity to the particle charge offers interesting analytical perspectives, and the device's nanoscale dimensions prefigure exceptional miniaturization potential.

Mass photometry is the latest methodology based on interferometric scattering video-microscopy.[9] It derives the mass of individual proteins and their complexes in solution from the intensity of the scattered light. Its simplicity and capability to analyze complexes in their native environment stir tremendous interest in the structural biology community, resulting in rapid adoption of the method.

A common feature of these three approaches is the acquisition of single particle data, which can be filtered and concatenated in the form of a particle mass distribution. We will review here the recent technological advances in single-particle mass analysis approaches.

Applications of CDMS in molecular biology and biotechnology have been the topic of a recent in-depth review, and the reader is referred to the excellent article by Martin Jarrold.[10] Consequently, although we will discuss applications to some extent, our primary aim is to provide a general view of the technological advances in single-particle mass analysis based on the interactions of a particle with electric fields, light, or vibrating nanostructures.

Charge Detection and Mass Spectrometry

Generalities

The earliest charge detection devices can be traced back to the mid-20th century with the advent of the Faraday cup for measuring high-energy electron beams.[11] In such a device, the

charged particles hitting an electrically insulated metal body are conducted to ground via an ampere meter, which measures the associated current.[12] The Faraday cup is the simplest and most commonly used destructive approach to measure the beam current directly. Charge detectors can be easily implemented with TOF-MS[13] and quadrupole ion trap MS (Figure 1a).[14]

On the other hand, image charge detection (ICD) is a non-destructive approach to characterize a charged particle in motion, and determine its charge, velocity, mass as well as other characteristics. Indeed, moving charges can induce a measurable image charge current as described theoretically by Shockley.[15] Simultaneous detection of charge and mass-to-charge ratio was pioneered by Shelton and co-workers more than 60 years ago with micron-sized particles with nearly 20,000 elementary charges.[16] Hendricks later applied the system to size oil droplets generated by electrohydrodynamic spraying.[17] A more sensitive device based on the Shelton design was then developed by Keaton et al.[18] and Stradling et al.[19] reaching a limit of detection of ~1500 charges. Another breakthrough in the analysis of high molecular weight compounds was made by the Smith group using a Fourier transform ion cyclotron resonance (FTICR) mass spectrometer to trap single ions of megadalton individual electrospray ions[20]. ICD is also used in other types of instruments, such as orbitrap mass spectrometers[6, 21], ion implantation systems[22], and specifically in charge detection mass spectrometry (CDMS) (Figure 1b)[5, 23].

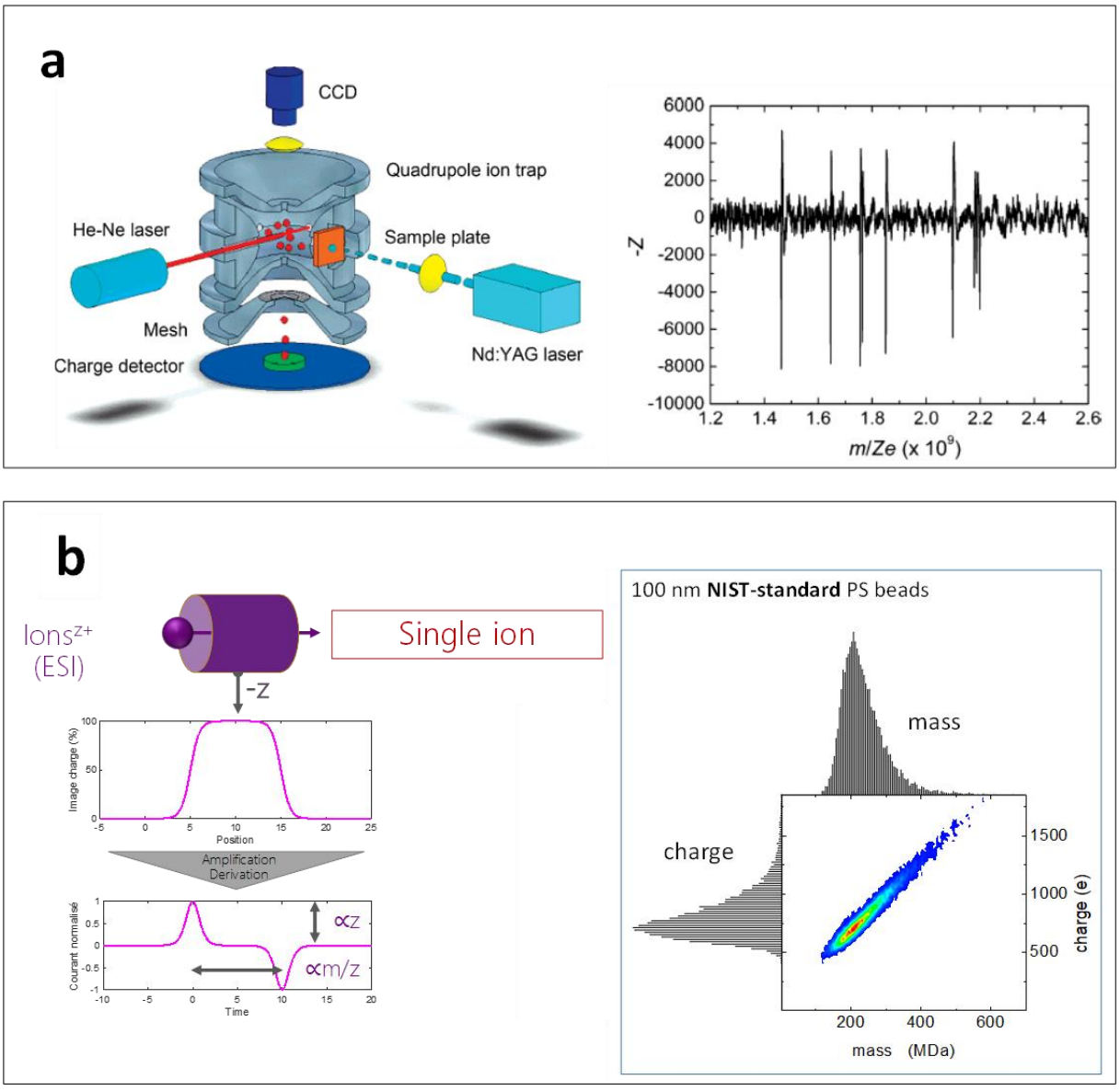

Figure 1: Various implementations of single particle mass spectrometry using destructive or non-destructive charge detection (a) destructive charge detection with a quadrupole ion trap from Chang's group (charge monitoring cell mass spectrometer). Reprinted with permission from ref.[24] (b) Principle of non-destructive single ion (image) charge detection time-of-flight mass spectrometry with a conductive tube. 2D mass-charge map for 100 nm NIST standard polystyrene (PS) beads.

Quadrupole ion trap with impact charge detection (CD-QIT MS)

This method typically combines a quadrupole ion trap (QIT) and a charge detector (

Figure 1a). The *m/z* is obtained by scanning the RF frequency applied to the quadrupole ion trap, and the charge is derived through signal integration as individual ejected ions hit the detector. Early developments of the technology were reviewed by Chang in 2009.[25] Shortly, Chang's group developed a single-particle mass spectrometer (SPMS) based on QIT-MS in 2002. To achieve an ultra-high *m/z* ratio and analyze submicrometer or nanometer-sized particles, they replaced the conventional MHz frequency power amplifier driving their QIT with an audio frequency (AF) system optimized at 50–2000 Hz.[26] In their setup, the *m/z* ratio of individual particles trapped in the quadrupole field was characterized by the ions' secular frequencies using an RF scan, and the charge accuracy was limited to several hundreds of elementary charges by electronic noise and the impact-based measurement approach. For these reasons, applications of impact CD-QIT-MS have largely focused on micrometer-size particles because those larger particles often carry more charges.[25] Building on their QIT-MS system with the incorporation of a laser-induced acoustic desorption (LIAD) ion source, Chang and Chen's group successfully measured the mass of 29.6 μm polystyrene microparticles up to $7{\cdot}10^{15}$ Da and were able to distinguish the mass distribution of cancer cells from normal cells.[27]

In 2017, Chen's group further incorporated an ESI ion source in their CD-QIT-MS design to measure different sizes of MCF-7 breast cancer cells (8 to 15 μm) with masses around 10^{14} Da.[28] The instrument was calibrated by a series of commercially available polystyrene (PS) microparticles with sizes comparable to cancer cells. In 2019, a new design of an open system interface allowed direct online analysis of continuous sample introduction for dry micrometer-sized particles with a mass limit of up to 10^{17} Da.[29]

Rooted in the impact CD-QIT MS setup, Peng's group increased the charging of analytes using a laser-induced RF plasma (LIRFT) ion source to surpass the limit of charge detection (LoD) from single particle impact in measuring submicrometer-sized particles in an alternative way.[30] They achieved this by experimenting with various reagent gases and gas mixtures to facilitate charge exchange reactions. As an example, the average charge of 0.75

μm polystyrene particles could reach 1631 e using an argon/methane mixture with a ratio of ~10:1. Based on this approach, they determined the average mass and charge of the vaccinia virus to be approximately $9 \cdot 10^9$ Da and 708 e, respectively.

More recently, Nie's group performed a so-called probe particle-based impact CD-QIT MS method to overcome the charge limit of detection (LoD).[31] In their setup, probe particles (e.g. 3 μm polystyrene particles) and target particles (493 nm to 1.6 μm polystyrene particles) were trapped together and simultaneously ejected from the QIT through flow ejection and resonance ejection, respectively. Following this coupled ejection, the smaller target particle's charge is superimposed on that of the larger probe particle, thus overcoming the LOD threshold. They successfully characterized the influence of enzyme encapsulation on single metal-organic framework nanocrystals by applying a visible-wavelength matrix-assisted laser desorption/ionization (MALDI) ion source.[32] The mass range was down to 10^{10}–10^{12} Da and the mass resolution was about 20.[33]

Currently, impact-based CD-QIT MS remains a superior method for rapid single-particle mass analysis in the ultrahigh mass range (above 10 GDa). Yet, impact-based CDMS charge accuracy suffers detection limitations that are mainly due to electronic noise (generally about a few hundred elementary charges) and the signal-to-noise ratio can hardly be further improved by remeasurement as it relies on a single-shot detection.[32]

Charge detection mass spectrometry (CDMS)

From Single to Multi-pass

The passage of a charged particle in the vicinity of a conductor induces a charge-image on this conductor (Figure 1b). For example, a positive ion entering an insulated conductive tube induces a negative charge inside the tube and a positive charge outside. The induced charges are maintained until the ion leaves the tube. When this happens, the induced charges dissipate. When the tube is long enough, the value of the induced charge approaches that of the ion charge. Under specific geometrical conditions, analytical solutions for calculating the

charge-image are derived using the Shockley-Ramo theorem.[15] At this stage, it is worth mentioning that the charge of an ion resulting from the addition or removal of elementary charges, is expressed as an integer multiple (z) of the elementary charge ($e = 1.602 \times 10^{-19}$ C). Based on the detection of the charge-image of an ion passing through a conductive tube, CDMS simultaneously measures the charge (z) and the time-of-flight (TOF) of the ion through the tube, which relates to its mass-to-charge ratio (m/z). From these parameters, the mass ($m = z \cdot m/z$) of individual ionized species from the sample of interest can be deduced.

In practice, highly charged ions produced by ESI pass one by one through a small cylindrical metal tube connected to a charge preamplifier which captures their image current. The detector tube is connected to the input of a charge-sensitive preamplifier through a field-effect transistor (JFET). The signal is processed with a Gaussian differentiator: an ion passing through the tube thus produces two pulses of opposite polarities as it enters and exits the tube (Figure 2a). A negative amplitude pulse corresponds to the charge imprinted on the cylinder as the positively charged ion enters the cylinder; a second positive amplitude pulse results from the ion leaving the cylinder. The amplitude of the charge-image signal is proportional to the total z charge of the ion. The mass of each ion is obtained as a combination of the m/z value and the charge. Charge detection measurements on several thousand individual ions enable mass distributions to be rapidly constructed.

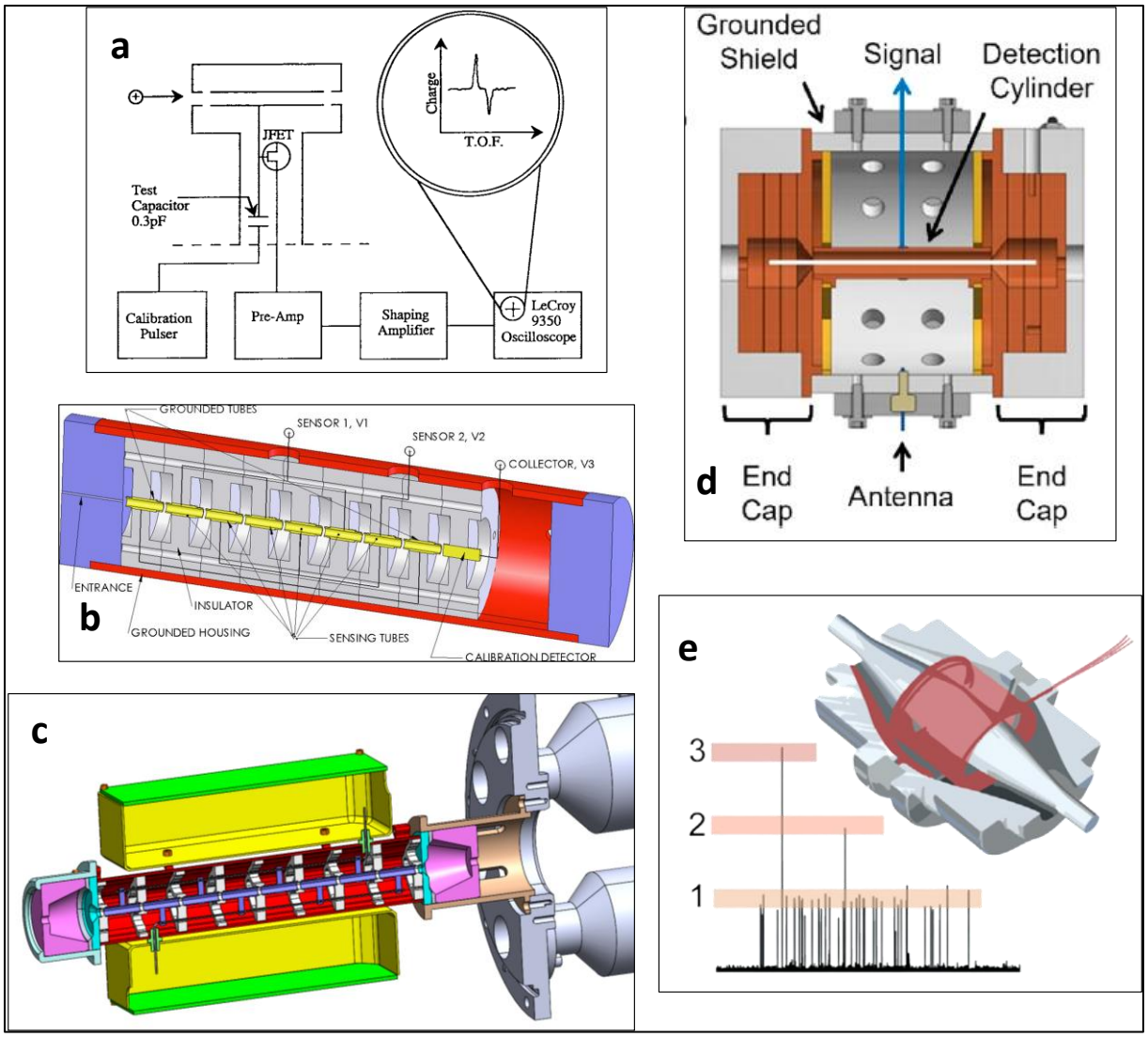

Figure 2: Different working modes of CDMS implementations including the original CDMS design by Benner in single pass (a), CDMS with multiple sensing stages (b) a multiple sensing stages combining trapping mode used in the ARIADNE platform (c) CDMS in trapping mode in its modern adaptation by Jarrold et coll. (d). Orbitrap-based CDMS version (e). Reprinted with permission from Refs.[10, 34-37]

Seeking to apply the time-of-flight technique to massive ESI generated ions, W.H. Benner and coworkers pioneered the development of CDMS technique. They established its proof-of-concept by analyzing DNA macro-ions and intact viruses with masses ranging from a few MDa to tens of MDa.[34, 38] To date, several research teams are active in the instrumental development of this technique. The teams led by M.F. Jarrold[39] and E.R. Williams[40] are developing charge detector arrays, as well as coupling with electrostatic traps to improve the

sensitivity and precision of this technique. D.E. Austin's team, meanwhile, is working on miniaturizing the technique using printed circuit boards.[41] Finally, R. Antoine's team is developing CDMS combination with separative techniques and laser spectroscopy.[23]

There are three CDMS detection modes (Figure 2 a-d) : (i) single-pass mode: a single ion travels through a single detector tube; (ii) single-pass using multiple sequential detectors: a single ion travels through an array of detector tubes; (iii) multi-pass using ion trapping mode: multi-pass of a single ion in a single tube. The single-pass mode is the most straightforward and features the broadest mass range (from 1 MDa to 1 TDa); the m/z ratio is determined from the time of flight through the tube (knowing the ion's kinetic energy). An in-house built single-pass charge detector has recently been constructed and mounted inside the vacuum housing of a commercial mass spectrometer (Micromass-Waters Quattro I, Waters Corp., Manchester, UK). This visualization of the most highly charged droplets (that bear numbers of charges near those defined by the Rayleigh equation) was exploited as a calibration aid for the charge detector, which lacks a means of precisely defining ion energy.[42]

However, the limit of charge detection (~250e), and the charge uncertainty (~50e) are constrained. Another approach to improve CDMS capability is to arrange charge detectors in series (Figure 2b). The charge is thus measured several times, which reduces the uncertainty in the charge measurement by a factor given by the square root of the number of measurements[43]. To further improve charge measurement, the detector tube (or the array thereof) can be integrated inside an ion trap, so the charge of an ion can be measured hundreds or even thousands of times as the ion oscillates back and forth in the trap. This CDMS mode is known as trapping mode (Figure 2d). In this case, the m/z ratio is usually determined from the ion's oscillation frequency (via Fourier transform analysis, FFT). Hybrid modes of charge detection mass spectrometers have recently been developed combining a tube detector array within a cone trap (figure 2c).[44] Ion trap CDMS is by far the most accurate CDMS mode, but it is also the most time-consuming. Single-pass CDMS is the least accurate but the fastest, while CDMS with in-line detectors lies between these two extremes. With

recent innovations in ion trap CDMS, it is now possible to measure charge with essentially perfect accuracy (see below).

Improving charge detection limits and accuracy

In their early work, Benner *et al.* used the ion detector signal to trigger trap closure, restricting the limit of detection (LoD>250 e). In contrast, Jarrold's group developed a new CDMS approach in 2013 called “random trapping mode” in which the ion mirrors of ion trap are held in their transmission modes for a selected time period during which one or more ions generated by the ion source will be expected to enter and travel through the CDMS device. This new CDMS design, enabling the measurement of much smaller signals, comprised an electrospray source coupled to a dual hemispherical deflection analyzer (HDA), followed by a modified cone trap incorporating an image charge detector, achieved a LoD of 30 elementary charges (e) and an average uncertainty of 3.2 e for single ion measurement.[45] A significant improvement was achieved by cryogenically cooling the junction field-effect transistor (JFET) located at the input of the charge-sensitive preamplifier that senses the induced image charge. This improved the transconductance and reduced thermal noise, resulting in a 1.7-fold increase in signal-to-noise (S/N) ratio. Consequently, the LoD was lowered to 13 elementary charges (e) with an RMS deviation of 2.2 e.[46] In 2015, Jarrold’s group further reduced the uncertainty of charge determination to 0.65 e with a LoD of 7e by optimizing several factors limiting the ion's trapping times, substantially extending the trapping up to 391 ms.[47] Furthermore, by lowering the background pressure by two orders of magnitude and extending the trapping time up to 3 s, they eventually reduced the uncertainty to below 0.2 e, an optimal value to enable correct charge attribution with 95% confidence while maintaining the measurement throughput.[48] Additionally, a novel scheme was employed to analyze experimental time domain data using harmonics to improve the signal-to-noise ratio and correct for variations in charge magnitude due to differences in ion trajectory and kinetic energy.[49] When the charge uncertainty is below 0.2 e, quantizing the charge (assigning it to the nearest integer state) is beneficial. Discarding ions with

intermediate charges reduces the charge quantization error rate to less than 1 in 15,000.[48] More recently, an implementation of a charge-sensitive amplifier without a feedback resistor for CDMS was reported, reducing noise and enabling the detection of individual ions carrying a single charge.[50] Besides, the Jarrold group developed a dynamic calibration of the charge measurement using an internal standard from a small antenna with a radiofrequency signal. This enabled the charge of an ion to be measured with a relative charge uncertainty of around $5 \cdot 10^{-4}$, allowing low-error charge-state assignment to be performed for ions carrying a charge of up to 500 e.[51] These recent advances provided high-accuracy charge measurements, improving the mass resolving power by an order of magnitude, and up to ~300 for 3 and 4 MDa macro complexes (T=3 and T=4 HBV capsids).[52] Significantly, these developments have made it possible to investigate previously intractable problems, such as the binding of small species (e.g., drugs and proteins) to much larger species (e.g., capsids and protein complexes).[10]

Multiplexing CDMS

One restriction of the original CDMS method is that only single ion trapping events were useful, as the presence of two or more highly charged ions during trapping events caused interactions that perturbed oscillation frequencies.[5] Therefore, to prevent the trapping of multiple ions, the transmitted ion current was adjusted to maximize the likelihood of having a single ion in the trap. As an unintended consequence, a significant fraction of an experiment was spent collecting data while no ions were trapped. In addition, *m/z* determination in trapped ion CDMS is sensitive to the ion's initial kinetic energy, thereby reducing the achievable mass resolution even with accurate charge measurement. This was solved by using energy filtering prior to trapping, which further reduced the experimental throughput by rejecting unsuitable analyte ions.[53]

In 2018, Williams' group investigated a method using higher-order harmonics of the CDMS ion signal to determine ion energy per charge.[54] The ratio of the fundamental frequency and second harmonic depends on the ion energy, which is an essential parameter for measuring

ion mass in CDMS.[49] Subsequently, this method was used to correct the influence of ion energy in *m/z* measurements by normalizing the fundamental frequency amplitude with the modeled amplitudes based on the design of cone-trap CDMS. This method removes the systematic changes during the measurement and enables an average of signal amplitude over long times, on which - the charge uncertainty can be reduced to +/-1 charge for a PEG ion with ~1000 charges with 500-ms measurement.[49] Moreover, they took advantage of the ability to acquire ion energies throughout the measurement process to enable the efficient weighing of individual masses of multiple ions trapped in CDMS that are indistinguishable from those trapped individually. They demonstrated a broad range of ion energies by maximizing the decoupling of ion *m/z* from the frequency domain, significantly reducing the rate of signal overlap. This approach allowed for an order of magnitude improvement in the time required to obtain a mass histogram with CDMS.[55] Additionally, trapping events with even more ions could lead to further gains in ion measurement efficiency.

Orbitrap-based image-charge CDMS

Single ion detection in FTMS

As pointed out earlier, Fourier transform (FT) mass spectrometers, whether based on Ion Cyclotron Resonance (ICR) or electrostatic ion traps like the Orbitrap (Figure 2e), also rely on image current detection for *m/z* and ion abundance determination.[56] While they conventionally detect ion ensembles, single ion detection has been previously demonstrated with FTICR and Orbitrap mass spectrometers.[57, 58] Such an approach was later shown to achieve greater sensitivity, resolution, and mass measurement accuracy for larger analytes. [59] However, early experiments on Orbitrap contented with *m/z* measurements and although it was conjectured, the potential of single ion charge determination was not immediately investigated.[58] A very interesting perspective on the early challenges and specifics of using FTMS for charge determination can be found in a recent article by Richard D. Smith.[60]

Charge determination in Orbitrap

In 2020, Kafader *et al.* and Wörner *et al.* independently reported new methods for correlating individual ion signals and charge states using Orbitrap Q Exactive UHMR™ instruments. Kafader *et al.* introduced an innovative approach called the selective temporal overview of resonant ions (STORI) process, based on assessing the induced current by an ion on the Orbitrap detection electrodes as a function of the acquisition time.[61] They extracted raw transient signals to correlate the ions' charge state with the slope of the integrated signal over the detection period as illustrated in Figure 3 for three hypothetical individual ion signals. The slope of the integrated signal in the STORI plot was found to be proportional to the charge of the ion. After a slope-to-charge calibration function, the mass of each ion could be determined using integer charge (z) and *m/z*, resulting in a spectrum in the true mass domain with increased resolution. They demonstrated the use of this approach, termed individual ion mass spectrometry (I2MS), over a range of masses from 8 kDa to 3.2 MDa.

Similarly, Wörner *et al.* observed a linear relationship between peak intensity and ion charge for single ions over a mass range from 150 kDa to 9 MDa.[62] In native-MS spectra, charge states of low heterogeneity samples are typically well-separated, and accurate charge states can be determined in the *m/z* domain, particularly with known mass standards. These determined charge states of standards can be used to correlate their peak intensities in the m/z domain, resulting from a single ion image charge, for appropriate calibration of signal intensity to charge factor. By comparing the assigned charge states to the single-ion intensities at the corresponding *m/z*, Wörner *et al.* constructed a calibration curve with an R^2 of 0.997, enabling the determination of individual ion's charge state with an r.m.s.d. of 3.5 charges.

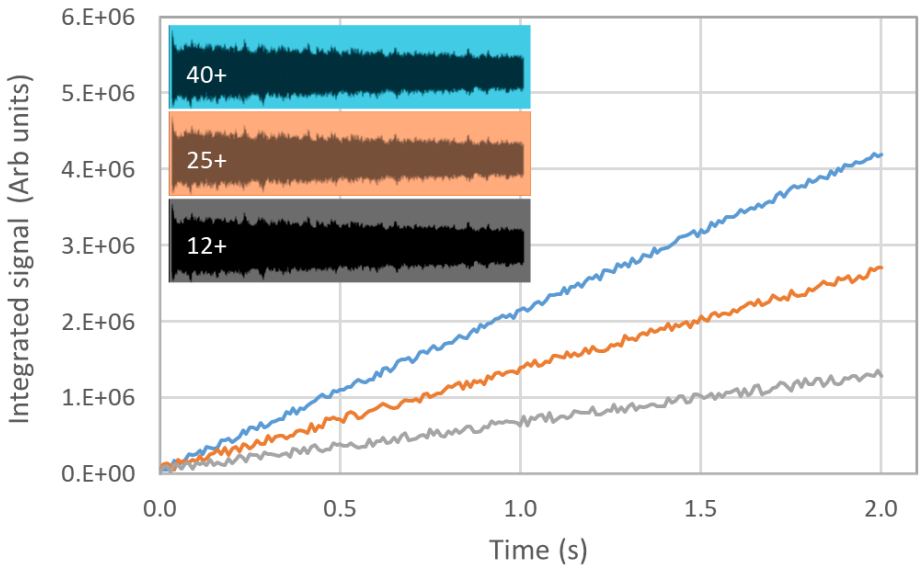

Figure 3: Simulation of Selective Temporal Overview of Resonant Ions (STORI) approach to derive charge information from single ion Orbitrap data. The integrated signal of a given ion over the detection period increases linearly, with a slope proportional to the ion's charge. Longer detection periods improve the charge accuracy. Note: Simulated time domain signals and their integration curves are solely for illustrative purposes and do not correspond to actual single ion signals.

Both I2MS and the peak intensity approach enable CDMS–like experiments on Orbitrap mass analyzers without requiring hardware modifications. These new methods improved the ability to determine the mass and charge of individual ions, and found a variety of applications in biological and chemical analysis. The inherent multiplexing ability of the Orbitrap analyzer, allowing many single ions to be trapped and detected simultaneously, and the reliance on signal accumulation to achieve high charge accuracy position this analyzer as an interesting complement to trapped ion CDMS approaches. The same attributes are being sought in innovative instrument designs such as the dual electric sector trap developed by Hoyes and Wray.[63]

Supporting Software

As the CDMS method has been independently developed by Heck and Kelleher's group on commercially available Orbitrap platforms,[61, 62] two divergent approaches and processing algorithms were developed to generate CDMS spectra from Orbitrap data. The reliance on customized codes in a few research groups initially hindered the spread of the technology. Building upon the STORI workflow,[64] Thermo Fisher Scientific now provides the Direct Mass Technology (DMT) mode commercially, offering accurate mass determination with charge detection capabilities. Although great advancements have been made in CD-MS measurements with Orbitraps, the standard deviations of the charge measurements are still 1–3 charges, which causes significant uncertainties in the mass. Custom instruments have achieved the highest charge resolution with uncertainties less than a single charge, but charge resolution can still be limited by the measurements in some cases. Marty's group developed an algorithm within the UniDecCD (UCD) software that enables fast deconvolution of two-dimensional (2D) CD-MS data to computationally reduce the uncertainties in charge assignment, dramatically improving the accuracy of CDMS data from Orbitrap detectors.[65] Moreover, this software demonstrated the capability of improving the CDMS resolution for proteins, megadalton viral capsids, and heterogeneous nanodiscs made from natural lipid extracts, which shows a great potential to advance CD-MS technology and expand its applications for large biomolecular complexes.[65]

Applications of image-charge CDMS

Besides occasional applications in large polymers[34, 49, 66] and solvent droplets[67, 68], large DNAs[69-71], nanoparticles[72-74], self-assembled nanostructures[75, 76], amyloid fibers[77-79], extra-cellular vesicles[80], or cells characterization[28], CDMS has pushed forward the envelope of mass spectrometry to analyze viruses and virus-like particles[81]. Applications of CDMS (both in trapping mode and in orbitraps) thus expand the range of top-down protein MS as well as native MS.

Antibody–antigen complexes

Qualitative and quantitative mass analysis of antibodies, antibody-antigen complexes, and related macromolecular immune complexes is a prerequisite for determining their identity, binding partners, stoichiometries, and affinities. Nevertheless, many of the targeting antigens are heterogeneous in composition and mass, which challenges conventional native MS methods due to the difficulties in resolving charge state distributions. Consequently, the mass of highly heterogeneous complexes can not be easily determined by native MS.[82]

Likewise, the spike protein trimer from the SARS-CoV-2 virus associated with potentially 66 N-glycan and 3 O-glycan sites is known to be highly heterogeneous.[83] Miller *et al.*estimated that spike protein trimer could present as many as 8.2×10^{75} glycoforms, which implies that the most likely glycoform of the spike trimer has a probability of only 1.9×10^{-34}. Therefore, the probability of two spike trimers having the same glycan distribution is vanishingly small.[84] Revealing individual masses from such broad combinations constitutes a formidable challenge for conventional native-MS methods. Interestingly, average glycan masses determined by "top-down" CDMS measurements were 35–47% larger than those obtained from the "bottom-up" glycoproteomics studies, suggesting that the glycoproteomic measurements underestimated the abundances of larger, more-complex glycans. Yin *et al.* applied CDMS methods on an Orbitrap Q Exactive UHMR™ mass spectrometer to measure full IgG binding to the trimeric SARS-CoV-2 S ectodomain.[85] Their experiments revealed that antibodies targeting the S-trimer typically prefer stoichiometries lower than the symmetry-predicted 3:1 binding ratio. Surprisingly, these substoichiometric complexes were fully effective at blocking ACE2 binding despite containing free receptor binding sites. These results highlight the importance of studying antibody/antigen interactions using complete, multimeric constructs and showcase the utility of single particle mass analyses in unraveling these complex interactions.

Ribosomal particles

Ribosomes are large ribonucleoprotein complexes responsible for protein synthesis through the translation of messenger RNA (mRNA). It has been shown that the composition and heterogeneity of ribosomes can vary significantly between different organisms and even within a single cell.[86] Such samples are highly challenging for mass analysis using conventional native MS. In 2021, Lai *et al.* analyzed intact ribosomes from various origins using an Orbitrap-based CDMS method, which enabled mass measurements of such large and heterogeneous biological systems.[36] Their samples included intact 80S ribosomes from human cells (Hs80S, ~3.8 MDa) as well as 70S chloroplast ribosomes from spinach (So70S, ~2.4 MDa). They also evaluated the limits of CDMS resolving power by separating Hs40S (~1.2 MDa) and the viral HCV IRES RNA-bound Hs40S (~1.3 MDa) particle, which showed an increase of mass by ~8% upon binding.

Viruses, Viral vectors, and Virus-like-Particles

In addition to the fundamental relevance of viruses in virology and epidemiology, recent advances in gene therapy and vaccination rely on viral vectors to deliver genetic or antigenic cargoes to specific cells. Thanks to their low immunogenicity, high transduction efficiency, long-term expression, low pathogenicity, and high safety profile Adeno-associated viruses (AAVs) are increasingly used as gene therapy vectors. AAVs package their genome in a non-enveloped T=1 icosahedral capsid of about 4 megaDalton. Notably, their capsid assembly from 60 subunits of 3 distinct viral proteins (VPs) is greatly divergent and stochastic, which is very challenging for conventional native MS methods because of their limited resolving capability.[87] Following previous work by Jarrold's group, who resolved AAV capsids containing the entire vector genome from those containing partial genomes and from empty capsids using the CDMS method,[88] Wörner *et al.* performed a detailed assessment of genome packaging in AAVs using commercial Orbitrap-based CDMS.[89] Their work subsequently enabled the exact quantification of production variability as well as the encapsulation efficiency of AAV vectors.[90] Only micro-liter quantities were required for the measurement

with a concentration level of about 1E13 viral capsids per milliliter. Besides viral vectors, Orbitrap-based CDMS has also shown the capability of measuring intact viruses and virus-like-particles (VLP) such as intact Flock House Virus (FHV; 9.4 MDa),[62] bacteriophage MS2 VLPs (1.0 and 3.1 MDa)[61] and engineered AaLS-neg nanocontainer (3.0 MDa)[62]. This commercially available scientific platform is attracting broad interest in the screening of viral samples.

Relatedly, Jarrold's group recently conducted a study exploring the use of CDMS for vaccine characterization, utilizing a custom-built CDMS system.[91] They successfully analyzed three widely used multivalent vaccines: IPOL (Sanofi Pasteur) containing whole-inactivated viruses, RotaTeq (Merck) incorporating live-attenuated viruses, and Gardasil-9 (Merck) composed of VLPs, with masses reaching tens of MDa. Notably, CDMS enabled the determination of the mass distribution of antigens and their assemblies, as well as the masses and relative abundances of impurities such as empty and defective particles. This robust technique eliminates the need for sample-specific standards, offering a valuable and versatile approach to vaccine analysis

Challenges and perspectives of CDMS

Conventional MS methods rely on transferring molecules from the condensed phase into the gas phase via ionization. Based on established native MS methodologies, CDMS measurements require buffer exchange into nano-ESI compatible solutions. This may result in method-specific biases that affect the quantification and detection of certain macromolecules, for which charge-independent MS technology (vide infra) can be complementary methods. Of note, Willams and collaborators developed a method enabling mass measurements of proteins and protein complexes directly from a variety of commonly used buffers with high concentrations of nonvolatile salts, therefore eliminating the need to buffer exchange into volatile ammonium buffers traditionally used in native mass spectrometry.[92] In addition, depending on the implementation, CDMS approaches may suffer from large uncertainty in the charge measurement that limits the achievable mass resolution.

Thanks to recent technological breakthroughs, overcoming the uncertainty associated with charge states and achieving unit charge resolution (0.2e) in detection has been achieved by Jarrold's group.[48] Unit charge resolution in CDMS has also been demonstrated by the Williams group.[93] However, analyzing only one or a handful of ions at a time means that conventional CDMS is slow. Each ion can be measured quickly, but many individual ions must be measured to build up a mass spectrum. John Hoyes is currently working on speeding up the process, by designing a CDMS instrument that swaps the linear configuration for a figure-eight path (Poschenrieder design).[94, 95] In this particular figure-eight path, the ions don't have to slow down to change direction at the end of a tube (as it is the case in cone traps[96] and Benner traps[97]). Another direction is to combine all modes of CDMS in a single instrument as developed by Antoine's group in the ARIADNE platform [https://cordis.europa.eu/project/id/964553/reporting][37]. Moreover, in the context of FT-MS data analysis for the CDMS approach, the monitoring of frequency drift in individual ions caused by desolvation and charge stripping leads to enhanced effective ion sampling, resulting in a twofold improvement in both mass precision and resolution.[98] Interestingly, a so far unvalidated report pointed out a method for charge determination analysis via advanced FT-MS data analysis by assigning charge state (z) to every ion peak, adding a new dimension to conventional m/z spectra.[99] Besides the analysis of very high MW species, CDMS has shown significant advances to conventional top-down MS in analyzing complex protein mixtures without chromatographic separation.[100] Charge detection mass spectrometry provides access to valuable information such as mass and charge distributions. However, no structural information can be derived from these distributions. By contrast, tandem mass spectrometry (MS/MS) is able to provide structural information. Typically, an excess of internal energy is deposited in the parent molecular ion, resulting in fragmentation. Antoine's group studied multiphoton infrared dissociation dissociation (IRMPD) of bacteriophage DNA in the MDa range.[71] Although proof-of-concept of fragmentation in CDMS instruments was demonstrated, an extension of MS/MS capability based on the CDMS

method for superior native top-down MS analysis from heterogeneous samples is not only a significant challenge but also an expected development in the near future.

Nano mechanical resonator-based MS (NEMS-MS)

While MS approaches, including CDMS, use the particle's charge as a handle to derive its mass, alternative single-particle mass measurement approaches that rely on direct mass determination using the particle's inertia have been proposed. It is the case of nanomechanical resonator-based MS.

Nanomechanical mass sensors

Generalities

Nano-mechanical resonators are vibrating nanostructures such as cantilevers, drums, or beams, which determine the mass of particles deposited onto their active surface via induced change in their resonance frequencies. These structures incorporate nanoscale mechanical elements, as well as electronics for sensing, actuation, signal output, and processing.

In 1993, the proof of concept of individual particle mass sensing was illustrated by Cleveland *et al.*,[101] who suggested a method to determine the spring constant of micro-fabricated cantilevers used in scanning force microscopy. to do so, they proposed to measure a cantilever's resonance frequency before and after the addition of single tungsten micro-particles onto its end. They concluded that "An interesting application of the mechanical system not yet discussed is its use as a nanogram scale." Shortly after, Thundat *et al.* also noted that "micro-machined cantilevers used in atomic force microscopy offer interesting possibilities as chemical sensors".[102] They went on to show that the resonance frequency of gold-coated cantilevers reflected the adsorption of mercury vapor onto their surface, a variation that was linked with the surface treatment.

Building on their pioneering work in nanosystems fabrication,[103] energy dissipation,[104] and electrical characterization,[105] Roukes' team at Caltech proposed the concept of NEMS-based

Mass Spectrometry (NEMS-MS) at the turn of the century. In 2004, they theoretically evaluated the mass resolution of NEMS[106] and experimentally demonstrated the mass sensitivity of NEMS at the attogram scale, highlighting near-term prospects for mass sensing of individual macromolecules.[107] In this seminal article, few ag mass resolution was demonstrated and the measurement of individual molecule mass was anticipated.

Beyond the technological challenges associated with ultra-small mechanical device fabrication, the realization of NEMS mass sensing entails achieving sub-nanometric displacement sensing at high oscillation frequency (MHz).[108] Resolving such challenges engaged physicists for over a decade and resulted in a variety of devices with enhanced performance, culminating in present-day sensors.[8, 109-112]

A critical aspect of NEMS mass sensing relates to the ability to derive the particle mass from the amplitude of the changes in device's resonance frequencies. Although several approaches have been proposed, each with specific advantages and limitations, this is still an active area of research.[113-116]

While initial demonstrations of NEMS mass sensing involved the observation of frequency discontinuities related to the deposition of a few particles, subsequent efforts aimed at performing mass measurement in real-time and on larger populations of particles to acquire particle mass distributions. One of the issues facing these measurements relates to the small particle capture cross-section of nanoresonators, and a variety of solutions have been explored over the years, ranging from enhanced particle guiding strategies[117, 118], resonators geometry[119], multiplexing using resonator arrays[120], or performing the measurement at ambient conditions[121], as we will see below.

NEMS resonance frequencies can in theory be sensitive to particle mass, position, stiffness, or even shape, depending on the resonator's dimensions, geometry, and modes of vibration. [117, 122] However, this requires monitoring additional resonance frequencies. The complexity of the measurement therefore escalates exponentially with the number of parameters involved,

and beyond two or three, it becomes very challenging to manage from an experimental point of view.[8]

Inserting a NEMS into an MS architecture.

In 2009, Naik et al. proposed to combine a nano-mechanical resonator with conventional MS-components.[123] They setup a hybrid system composed of an atmospheric pressure ion source and a series of differentially pumped ion transfer multipoles to convey electrosprayed protein ions to a resonant NEMS operated at 40K. The device was a 1.7µm by 120nm doubly-clamped silicon carbide beam coated with aluminum and titanium, with a quality factor of ~2000. They achieved a mass sensitivity of 12Hz/zg and a mass resolution of 17zg (10kDa). Using this setup, they could record events associated with the adsorption of individual Bovine Serum Albumin (66kDa) and β–amylase (200kDa) ions. However, because the magnitude of the observed frequency jumps also depended on the landing position, the mass of individual molecules could not be directly determined. Instead, the authors accumulated enough individual particles to achieve quasi-homogeneous deposition over the resonator's surface and through comparison of the observed distribution in frequency shifts with the theoretical one, they were able to deduce a mass distribution. They thus concluded that frequency jumps observed during the acquisition could be attributed to the adsorption of single protein ions.

First bio-molecular mass spectrum

In 2012, Hanay *et al.* demonstrated the first nanomechanical mass spectrometry of single biological molecules in real-time, by monitoring multiple resonance modes of doubly-clamped silicon beam resonators.[113] Using these devices, monitoring the first two resonance frequencies was required to deduce the mass and the position of deposited molecules. Since frequency fluctuations in the two modes translate into uncertainties in mass and position, an error model was devised to compute the Joint Probability Density Function of particle mass and position relative to frequency noise, thereby defining a mass resolution for individual particle landing events. Using these devices, they acquired mass spectra of gold nanoparticles

desorbed by MALDI and of electrosprayed human Immunoglobulin M complexes in the 0.5-2.5 MDa mass range.

MS of neutral species using NEMS

Benchmarking NEMS-MS with TOF-MS

At this point, no direct comparison of nano-resonator mass sensing with conventional mass measurement had been reported. In 2015, Sage *et al.* described an experiment in which a doubly-clamped beam nano-resonator was inserted in front of a custom time of flight (TOF) instrument equipped with a metallic cluster source.[124] Using this setup, they confirmed the consistency between mass measurements obtained using both methods. Moreover, using a deflecting voltage to remove ions from the particle beam, they showed that NEMS could detect uncharged particles, experimentally demonstrating the charge-independence of nano-resonator mass measurements for the first time. Nano-resonator-MS resulted in simplified mass spectra, since species with different charges appeared as a single peak, allowing the detection of neutrals to which the TOF was inherently blind.

Multiplexing the measurements

In order to multiply the capture area of the highly sensitive but small mass sensors, Sage *et al.* reported on the development of nanoresonator arrays associated with a dedicated readout scheme to probe each device sequentially.[125] They demonstrated the ability to control such arrays with a simple routing and a reduced number of electrical connections, with the same number of input/output (I/O) ports as a single device. In their design, the input signal was applied to the whole array while the output was the sum of individual resonator's contributions. Retrieving information corresponding to each resonator within the array was performed by "frequency addressing": distinct resonance frequencies for each resonator were obtained by slight variations in the designed sensor's length. Each individual resonator could thus be identified by its own resonance frequency and monitored separately, provided its frequency was sufficiently separated from that of other devices within the array. A main

advantage of this approach was that operating devices within the array did not degrade mass resolution. The authors highlighted the potential of such nano-resonator arrays for gas and mass sensing applications.

Subsequently, Sage *et al.* demonstrated using arrays of 20 multiplexed nanomechanical resonators in an MS setup.[120] Mass spectra of metallic aggregates in the MDa range were acquired with more than one order of magnitude improvement in analysis time compared to individual resonators. The 20 nano-resonators array was probed in 150 ms with the same mass limit of detection as a single device. Spectra acquired with a conventional TOF mass spectrometer in the same system showed excellent agreement in measured particle mass distributions. The authors also demonstrated MS imaging on the array at the single particle level, by mapping a 4-cm-diameter particle beam in the MDa range.

Dedicated neutral NEMS-MS system architecture

A significant milestone in NEMS-MS system architecture was proposed by Hentz and Masselon.[126] Their original arrangement of nanoresonator-MS departed from prior setups in that it did not rely on ion guides, but instead used aerodynamic focusing to guide particles to the resonator's active surface (Figure 4a).[118] This setup took advantage of the fact that nano-resonators are insensitive to charge, and inherently act as both a detector and an analyzer. It combined nebulization of analytes from solution, efficient particle transfer and focusing using an aerodynamic lens, and mass measurement of individual species using a nano-resonator array.

Independently, Malvar *et al.* also presented a NEMS-MS system without ion guides, with relaxed pumping requirements.[117] Their system consisted of three chambers with decreasing pressure: an ESI chamber operating at ambient pressure, a heated capillary chamber operating at 10 Torr, and a resonator chamber operating at 0.1 Torr. The NEMS resonator was placed 18 cm below the ionization source, which is an 11-fold increase in compactness compared to the prototype presented by Naik et al.[123] Their work showed significant improvement in decreasing the apparatus size, pumping requirements and complexity of the

system. However, their prototype was characterized by a small capture efficiency and consequently a low event rate, and on average 1 particle was detected every 200 s.

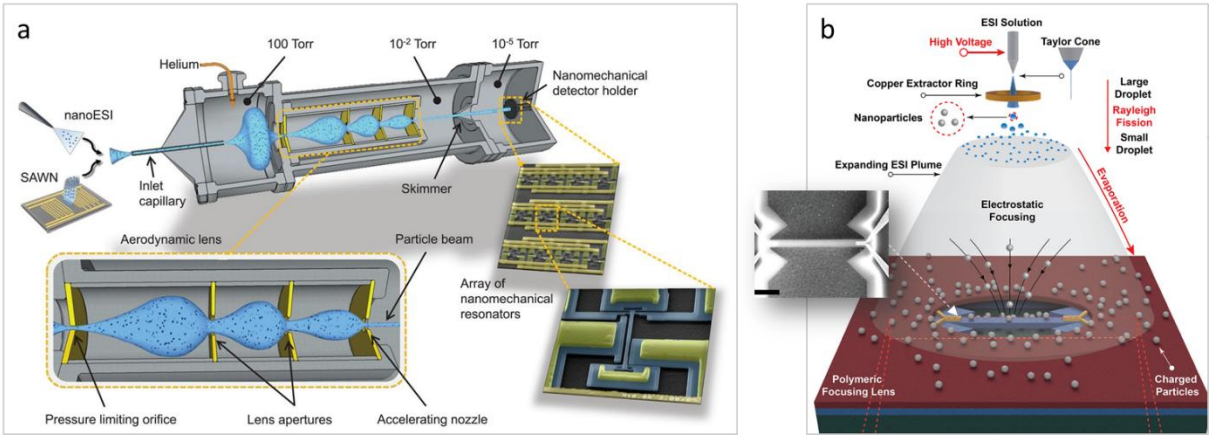

Figure 4: Recent NEMS-MS system architectures: Ion guide-free system with aerodynamic focusing of particles onto an array of 20 doubly-clamped beam resonators (a). Direct electrospraying and electrostatic focusing of particles onto a doubly-clamped beam at atmospheric pressure (b). Adapted with permission from Refs [118, 121]

In 2018, following a thorough assessment of their system's transmission and focusing capability using polystyrene nanoparticle standards, Dominguez-Medina et al. demonstrated the capabilities for analyzing bacteriophage T5 capsids, showing that the capsid with the viral genome has a theoretical mass of approximately 105 MDa, while the capsid alone (without the viral genome) has a theoretical mass of approximately 26 MDa. With the proposed MS architecture, the inertia of massive particles was exploited for efficient guiding and focusing using aerodynamic forces rather than having to be counteracted by electromagnetic fields (Figure 4a). This system was able to analyze individual particles regardless of charge, and overcame limitations associated with earlier nanoresonator–based systems using ion guides, in particular with respect to detection efficiency.[118]

NEMS-MS at atmospheric pressure

In another attempt to circumvent the small particle capture cross-section of nanoresonators, Erdogan *et al.* recently proposed a novel approach in which a solution containing the analyte

particles was directly electrosprayed in front of a nanoresonator at ambient pressure (Figure 4b).[121] To achieve enhanced capture efficiency, they devised a patterned photo-resist layer above the resonator. The charging of this layer through a collection of the first incoming ions from the electrospray caused electrostatic focusing of subsequent charged particles toward an open slit above the active area of the resonator. They validated their system using standard 20 nm and 40 nm gold, and 100 nm polystyrene nanoparticles. The mass distribution maxima were 71, 274, and 400 MDa, corresponding to diameters of 22.7, 35.6, and 106 nm, respectively, assuming spherical shape and uniform density. The size histograms were in excellent agreement with those derived from SEM measurements. Using this setup, they were able to improve the capture efficiency of nanoparticles by a factor of 100 compared to previous systems with the resonator under vacuum. However, this improvement was achieved at the cost of a significant drop in mass resolution (3.3 MDa) due to interactions of the device with the surrounding gas. They also applied this technology to the analysis of viral particles of BoHV-1 and SARSCoV2 inactivated by heat. In 2023, the same team further explored atmospheric pressure systems with a paddle NEMS devices using single-mode detection.[127]

Optomechanical mass spectrometry

Previously, nano-resonator MS systems relied almost exclusively on one-dimensional structures such as beams and cantilevers vibrating with flexural modes. The use of such devices with low capture cross-section forced a trade-off between analysis time and mass resolution: Larger devices present increased particle capture cross-section but at the cost of lower mass sensitivity. In addition, elaborate readout schemes are required to simultaneously monitor multiple resonance modes, which in turn degrades resolution. These issues restrict the applications of nano-mechanical MS.

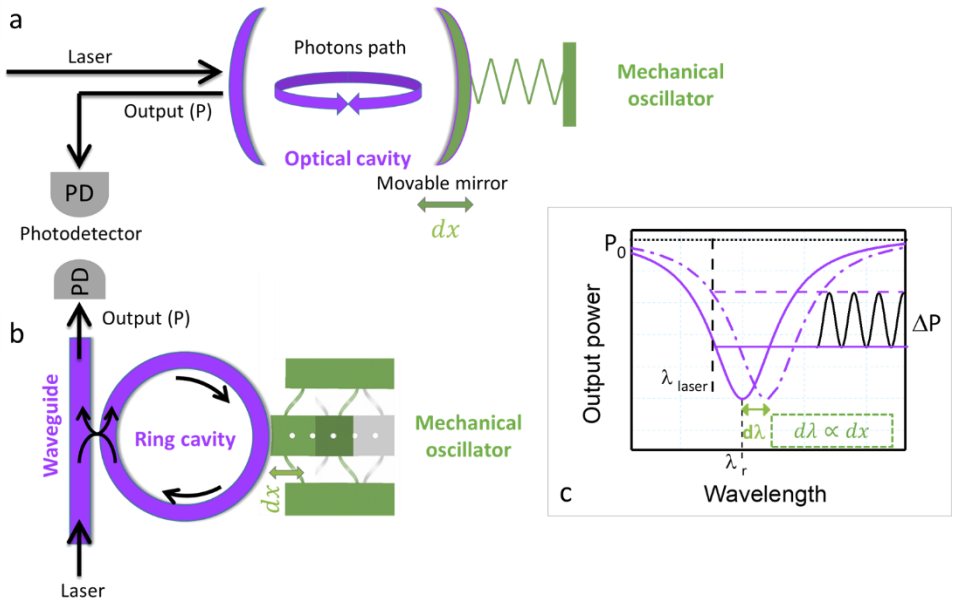

664

665 *Figure 5: Similar to a Fabry-Perot interferometer, that determines differential changes in*
666 *distance between two end mirrors (a), an optical ring cavity can be used to sense the*
667 *displacement of a mechanical oscillator in its vicinity (b). Oscillations of the platform*
668 *translate into periodic changes in the resonance wavelength, which can be measured at the*
669 *output of the waveguide through changes in the power of the transmitted light (c).*

670 Cavity optomechanical systems rely on interactions between light and mechanical resonators
671 (Figure 5a). These systems provide ideal platforms for precision sensing of various physical
672 quantities (e.g. force, mass, acceleration), due to the enhancement of both mechanical and
673 optical resonances.[128] In 2020, Sansa *et al.* demonstrated for the first time single-particle MS
674 with optomechanical nanoresonators.[119] For this purpose, they developed a "nano-ram"
675 resonator consisting of a 1.5 µm by 3 µm sensing stage supported by four 80 × 500 nm beams
676 (Figure 5b). In this device, the mass-sensitive platform oscillates in the plane as a rigid body,
677 i.e. without distortion of its surface. In doing so, it comes close to a 20 µm diameter ring
678 optical cavity, interacting with the evanescent light coupled into the cavity. Thanks to the
679 geometry of the device and its mode of operation, the frequency shift induced by a particle
680 landing on the platform is totally insensitive to the particle's position, stiffness, shape, or
681 aspect ratio. This scheme thus enables single-mode operation, significantly simplifying

682 readout and data processing. Importantly, mass sensitivity remains constant, and resolution
683 optimal over the entire sensing area, and the larger capture area yields faster acquisition.[119]

684 Using this device, Sansa *et al.* performed MS analysis of tantalum nanoclusters ranging in
685 mass from 2.8 to 7.7 MDa in <5 minutes, demonstrating good agreement with TOF-MS
686 measurements within the working range of the TOF system. They also demonstrated
687 excellent stability of the sensor during these experiments. This demonstration of on-chip
688 optomechanics as a superior alternative to electromechanical resonators for high-resolution
689 single-particle MS paved the way to high throughput analysis of synthetic and natural
690 nanoparticles, independently of shape, charge, or mechanical properties. For this purpose,
691 photonics-derived fabrication processes could be easily amenable to multiplexing using
692 standard telecom wavelength-division multiplexing and packaging techniques.

693 ## Towards NEMS-MS Applications

694 While most research in NEMS-MS has so far focused on proof of concept measurements,
695 access to mass produced reproducible devices has been a major hurdle preventing broader
696 applications. As devices fabricated with Very Large Scale Integrated Circuit (VLSI)
697 technologies are becoming available,[125, 129] this obstacle is gradually being lifted. We will
698 highlight here some prospective applications of NEMS-MS derived from recent reports.

699 In 2016, Malvar *et al.* determined the mass and stiffness of 100 nm gold nanoparticles and
700 intact E-coli bacteria using 100 nm-thick silicon nitride microcantilever with multimodal
701 detection.[117] They developed a theoretical framework to determine the analyte's position,
702 stiffness, and mass from the amplitudes of four resonance frequency discontinuities
703 corresponding to four flexural vibration modes. For the microcantilevers used in this study,
704 neglecting the effect of stiffness led to an underestimation of the mass of the bacteria by up to
705 10%. Their estimate of E-coli cells' Young's modulus at 4.2±1.0 GPa was consistent with those
706 obtained by atomic force microscopy (AFM). The authors stressed that describing the
707 analytes by two orthogonal coordinates, mass, and stiffness, could improve measurement's
708 selectivity, opening the door to original biomedical applications.

Dominguez-Medina *et al.* analyzed bacteriophage T5 capsids free of the viral genome and similar capsids with the viral genome at 27 and 105 MDa respectively using an array of doubly clamped beams.[118] Empty and filled capsids at concentrations of ~$5.9 \cdot 10^{11}$ and ~$8.8 \cdot 10^{10}$ particles·ml^{-1} respectively, were electrosprayed from 12.5 mM ammonium acetate solution spiked with methanol (10% v/v) for spray stability. The obtained mass distributions were centered within 2.5% of the expected masses, and the peak widths were broader than the instrument resolution, suggesting mass heterogeneities related to salt adducts. As a matter of fact, the presence of intercalated sodium atoms within the dsDNA viral genome could in itself account for as large as a ~2.5 MDa mass discrepancy if not taken into account. This work was later followed by a systematic assessment of the factors influencing the mass measurement in this specific implementation of NEMS-MS.[130] The conclusions were that the major sources of uncertainties related to the device's fabrication discrepancies, and that mass imprecisions due to frequency noise were on the order of ~ 0.1 MDa. More recently, Lai *et al.* assessed the potential of NEMS-MS for nanoparticle characterization.[131] Nanoparticles exhibit size-dependent properties that determine their physical behavior and interaction with the environment. Thus, particle size distribution is a critical parameter directly related to their practical applications. Typically, light scattering as well as imaging approaches are used as a means to estimate nanoparticle size and morphology. However, sizing methods often suffer from limited 1- or 2-dimensional descriptors and are ill-suited to analyze non-spherical or heterogeneous particles. To overcome these difficulties, particle mass distribution (PMD) can complement conventional NP characterization data. Following NEMS-MS analysis of nanoparticle samples, Lai *et al.* showed how PMD could help to infer particle density, corroborate polymer grafting and reveal heterogeneities of non-spherical particles (see Figure 6).[131]

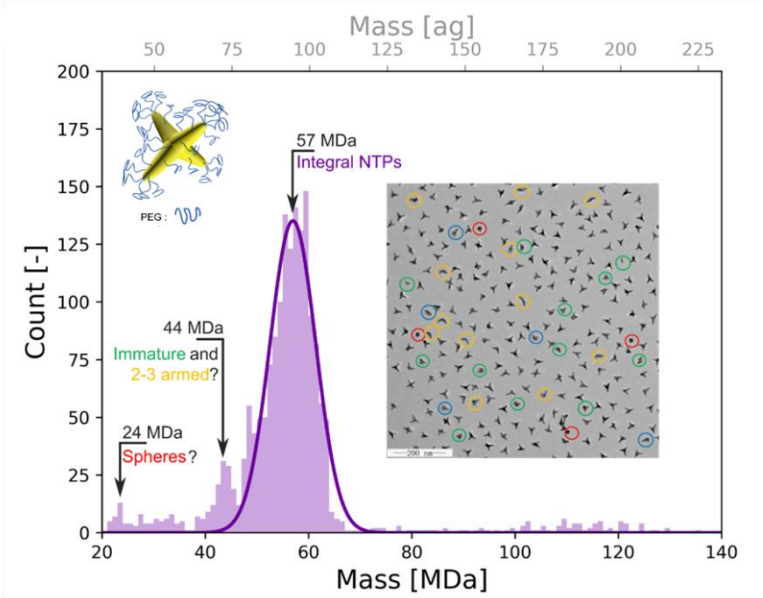

Figure 6: Particle mass distribution of poly-ethylene glycol grafted gold nano-tetrapods (top inset) obtained by ESI-NEMS-MS. The intact mass corresponds to the mass of gold as determined by ICP-MS plus that of PEG as determined by NMR. Evidence for deficient structures was confirmed by transmission electron micrograph (right inset). Adapted with permission from Ref [131].

Challenges and Perspectives of Nanoresonator MS

Importantly, while conventional MS displays resolution inversely proportional to masses, the resolution of nano-resonators-MS solely depends on frequency noise and remains constant over the whole dynamic range, making this technology more efficient as masses get larger. In addition, unlike conventional MS, nano-resonators do not require charging of the analytes, and the ability to use neutral injection methods will ultimately allow the direct monitoring of biological processes in real-time.

At this stage, NEMS-MS still lags CDMS in terms of analytical performance. Yet, NEMS-MS is still quite recent and remains under-developed, and continuing progress in resonator design, measurement multiplexing, or system architecture will undoubtedly unlock enhanced

analytical capabilities in the future. In this context, recent developments in optomechanical devices present interesting perspectives.

Mass Photometry (MP)

Weighing molecules with light.

In the same way as CDMS uses charge, and NEMS-MS exploits vibrations, a new technology termed mass photometry emerged recently, which relies on the interaction of light with a particle in solution as a means to characterize its mass.

Interferometric scattering microscopy

The capacity to perceive nanometer-scale objects and molecules with visible light has progressed substantially over the past decades.[132] Previously, single-molecule imaging relied almost entirely on fluorescence labeling as a contrast agent to distinguish the labeled compounds of interest from interfering species. Instead, extinction detection directly depends on the difference in the quantity of light transmitted by a sample in the presence and absence of the object of interest. However, imaging non-fluorescent particles at such levels of sensitivity entails discerning light having interacted with the particle of interest from intense background light. Even though a single molecule or even an atom can be detected in this way, the interference contrast in transmission does not exceed a few parts per million, requiring sophisticated noise suppression approaches.[133]

There have been several implementations of detecting linear scattering signals from single particles via interference, including interferometric scattering (iSCAT) microscopy[134, 135] and iSCAT in transmission geometry, known as coherent brightfield (COBRI) microscopy[136]. By detecting linear scattering light through interference, iSCAT microscopy is extremely sensitive, making it possible to detect single biomolecules; for instance, streptavidin as small as 55 kDa can be directly visualized[137]. Scattering-based light microscopy has been the subject of a recent in-depth review, and readers are referred to the excellent article by Kukura and collaborators.[132] Consequently, while we will discuss some applications, our primary aim is to

focus on the recent advances in commercially available instruments (Refeyn Ltd., UK) based on iSCAT technology for single-particle mass analysis.

Mass photometry

In 2017, building on prior developments in interferometric scattering microscopy (iSCAT), Kukura *et al.* proposed intercalating a spatial mask with partial transmission in the vicinity of the back focal plane of a high numerical aperture objective (Figure 7).[9] This feature improved the extinction scattering contrast at the image plane by a factor scaling with the mask's transmission coefficient. They hence demonstrated numerical-aperture-shaped interferometric scattering microscopy as a general approach to increase extinction contrast, enabling label-free imaging down to the single-molecule level. Further improvements in measurement sensitivity led to the development of mass photometry, a video-microscopy based method to determine the mass of individual molecules in solution knowing the relationship between the scattered light intensity and the object's size and density.[138]

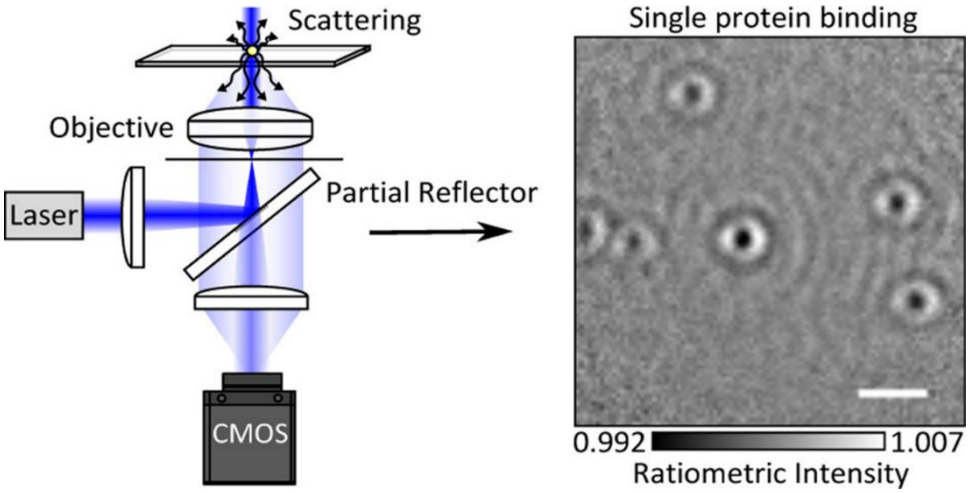

Figure 7: Mass photometry principle: A partial reflector placed in the vicinity of the back focal plane of a high numerical aperture microscope objective enhances the extinction contrast of particle scattering. Molecules landing onto the glass slide are detected through comparison of an instantaneous time-averaged image with a fluctuating background corresponding to the average of the preceding frames. Reprinted with permission from [9].

In the first implementation of this method, molecules landing onto a glass slide were detected through comparison of an instantaneous time-averaged image with a fluctuating background corresponding to the average of the preceding frames. Upon selection of a suitable integration period, landing molecules appeared as dark spots on the subtracted image upon landing, and disappeared moments later as their signals became part of the subsequent background image. The mass of each particle could then be derived by fitting the detected signal intensity with a model point spread function. The simplicity of mass photometry makes it an elegant and fast method to derive mass distributions of biomolecules in native conditions from minute sample amounts.[139]

Mass Photometry Applications

Owing to its speed, sensitivity and ease of use, MP rapidly found broad applications in structural biology and biopharmaceutical research for sample quality control, oligomerization studies[140, 141], interaction binding analyses of proteins[142, 143], nucleic acids[144], protein-nucleic acid interactions[145], antibodies[146], antibody-antigen complexes[82, 85] and viral particles[90, 147]. Also, size distributions of gold nanoparticles in solution were measured by single-particle mass photometry.[148] More recently, the first characterization by mass photometry of nanoaggregates of atomically precise nanoclusters in solution was reported by Wysocki and Pradeep.[149] We will focus here on three key applications of the method: the evaluation of the heterogeneity of proteins and their complexes, the analysis of membrane-associated proteins, and the characterization of viral vectors.

Quantify the heterogeneity of proteins and their complexes

The primary application of MP is the characterization of protein sample heterogeneity. Homogeneity is an important prerequisite to study protein function and regulation in order to avoid spurious interactions in the system of interest. Arguably, it is even more critical for structural analysis by crystallography or cryo-electron microscopy, as these technologies are especially sensitive to minute amounts of contaminants. In 2020, Sonn-Segev *et al.* benchmarked MP capability to quantify the heterogeneity of macromolecular complexes

samples by comparing its performance with negative stain electron microscopy (nsEM), a reference method for EM sample screening.[150] They demonstrated that MP-derived sample composition closely agreed with nsEM results, while offering specific advantages, including higher sensitivity, faster readout, and the ability to perform the analysis in native conditions. In addition, MP provided direct access to the diversity of sub-assemblies present in the sample by revealing the masses of all detectable species, without prior knowledge of sample composition. Importantly, it can do so in a time-resolved manner, allowing real-time studies of protein oligomerization in native solutions.[151]

Concurrently, Soltermann *et al.* demonstrated that MP could derive relative abundances of biomolecules and their complexes in mixtures via label-free single-molecule counting.[139] Analyzing mixtures of the monoclonal antibody trastuzumab with soluble domains of IgG Fc receptors or ErbB2 antigens, they determined the binding constants as a function of pH (over 4 orders of magnitude) and the associated binding kinetics of supramolecular assemblies having complex stoichiometries (up to 6 interacting partners).

Stalking membrane-associated proteins

Membrane-associated proteins are essential for many biological processes such as signaling, transport, or adhesion. Thanks to their specificity and accessibility, several of them are of high interest as drug targets. However, their hydrophobic regions, and association with heterogenous lipids, severely challenge analytical methods. Recently, a novel data processing approach to track individual membrane-associated proteins diffusing on supported lipid bilayers (SLB) using MP was independently proposed by two groups. This approach, termed dynamic MP[152] or mass-sensitive particle tracking (MSPT)[153], relies on a sliding median background processing method, which circumvents the convolution of scattering contrast and particle motion inherent to the conventional MP background subtraction. Application of dynamic MP to dynamin 1, a large GTPase catalyzing membrane fission during clathrin-mediated endocytosis, revealed heterogeneous mixtures of dimer-based oligomers, their respective membrane affinity as reflected by their residence time, and oligomer-dependent

dynamics, with a spatial and temporal resolution on the order of few nm and ms respectively. In this study, the observation of dynamin multimers with two, six, or ten copies of the protein on SLB, confirmed that, contrary to solution conditions in which dynamin exists primarily as a tetramer, surface oligomerization proceeds by the addition of dimers.[152] MSPT was applied to analyze the membrane-associated Min system, a three-protein system essential for the spatiotemporal regulation of cell division in E. coli. The authors reported the stoichiometry and turnover of individual membrane-bound MinD/MinDE protein complexes and quantified their size-dependent diffusion.[153]

Characterizing viral vectors

In the earlier discussion of the application of viral vectors in charge detection mass spectrometry (CDMS), we emphasized the widespread use of adeno-associated viral (AAV) vectors in gene therapy, owing to their stability, low immunogenicity, and non-pathogenicity. Recent advancements in mass photometry (MP) have showcased its capacity to distinguish and quantify various capsid populations within AAV particles, including empty, full-genome, and partially packaged capsids.[147] This capability is pivotal for ensuring the purity and safety of recombinant AAV (rAAV) preparations, given its rapid, robust, sensitive, and cost-effective nature. Furthermore, studies have demonstrated that both MP and CDMS can effectively resolve heterogeneous pools of AAV particles, spanning different serotypes such as AAV8 and AAV2, and revealing diverse particle distributions resulting from distinct production methods.[90] Additionally, MP has proven useful in accurately assessing genome length in AAVs through various calibration approaches.[154] Notably, recent investigations utilizing MP have provided insights into the thermal stability of AAV preparations. The study revealed that empty AAVs are more heat-resistant than genome-filled particles and indicated that capsid aggregation or disintegration occurs upon DNA release, rather than transforming into empty AAVs.[155]In summary, MP measures full, empty, and partially packaged capsid ratios, assesses genome length, and provides information on sample heterogeneity and aggregate presence. These collective findings underscore the potential of MP, alongside complementary

techniques like CDMS, in bolstering the characterization and quality control of AAVs for gene therapy applications.

Challenges and Perspectives of Mass Photometry

MS analysis is achieved through ion manipulation under relatively strong electrical or magnetic fields for ionization, desolvation, and *m/z* separation. Such handling can sometimes induce sample deterioration, which can potentially cause erroneous mass analysis. Compared with conventional MS-based methods, solution-phase-based MP methods circumvent the need for high voltages and additional sample preparation such as buffer exchange to maintain a native environment during data acquisition.

A side-by-side comparison of MP and CDMS was reported by Lai, Tamara and Heck, who analyzed ribosomal particles with both methods, using native MS as a reference.[36] Considering ease of use and sample consumption, MP appeared to be the method of choice to assess supra-molecular protein assemblies. However, CDMS provided better resolution and improved statistics, thanks to the higher number of detected particles per experiment and the reduced intrinsic mass measurement error. Interestingly, both methods eventually provided similar mass accuracy (< 1%) in the studied mass range (1-4 MDa). Nonetheless, it remained challenging for MP to achieve resolution and accuracy of mass determination comparable with MS-based approaches. In addition, MP heavily depends on the quality of the contrast-to-mass calibration, and the properties of interference reflection and interferometric scattering, which can be complicated, are not universal for different types of samples.[90]

On the contrary, the CDMS method features a more precise and universal charge-determined calibration along with a higher number of detected particles per experiment that enables the reduction of intrinsic mass error. Besides, CDMS depends on two-component analysis in both *m/z* and z-space, which provides an additional dimension for data analysis, boosting accuracy and resolution, and potentially separating overlapping signals in one dimension. To date, both methods are powerful single-particle mass analysis techniques undergoing fast development and expanding into numerous applications.

Conclusion and Outlook

Following the rise of biological MS, scientists are progressively coming to grasp the parts list of biological systems. They are thus gradually shifting their attention to determining how these parts assemble to carry out functions This entails switching from cataloging the basic components of living systems (proteins, nucleic acids, metabolites) to observing nano-biological entities in action. This in turn requires analytical methodologies to probe their assembly and dynamics.

Mass is a universal property of matter that has demonstrated capabilities to characterize and classify biomolecules composed of thousands of atoms. Yet, native-MS is challenged by the heterogeneity of heavier assemblies. In this context, recent advances in CDMS are opening new avenues to study such large biomolecular ions analogous to nanoparticles. Although commercial options are limited, new products are expected soon. For instance Megadalton Solutions[https://megadaltonsolutions.com], (founded by Jarrold, Benjamin Draper, and David Clemmer) offering CDMS as a service, recently worked to license the CDMS intellectual property portfolio to the instrument maker Waters. TrueMass (John Hoyes's company, https://www.truemass.co.uk/about-us), is in a similar situation, developing the first commercial CDMS instrument to support the analysis of macromolecules. As we explore this high mass range, we also encounter alternative approaches that do not necessarily rely on particle charge to assess their mass. Thus, mass can also be determined from the interactions of a particle with light or with a vibrating nanostructure. While these alternative approaches bring specific advantages and limitations, they have still to reach their full potential.

Importantly, all these methods analyze particles one at a time, which gives rise to multiple challenges: first, it takes time to analyze particles one by one; next this often involves rejecting data points for which the properties that lead to mass could not be properly measured, which may lead to selection biases; finally, in the upper mass range of interest, the resolution is not necessarily instrument limited, but relates to the sample composition.

Possible solutions to these issues have been proposed such as multiplexing the measurement using several detectors or measuring many frequencies, resorting to smart data processing approaches, or interfering with sample heterogeneity. Recently, Jarrold and coworkers reported the development of a post-processing method called multiple ion charge extraction (MICE) that uses a statistical approach to assign charges to ions with overlapping frequencies. High-throughput CD-MS with the MICE algorithm is the fastest and highest resolution method to analyze megadalton-sized particles.[156] In addition, CDMS has the potential to revolutionize mass spectrometry of complex mixtures. A spectrum that would be horrendously complicated due to overlapping m/z charge states can be resolved thanks to the independent measurements of mass and charge at the single-particle level.

The use of nanomechanical oscillators involves a trade-off between analysis time and mass resolution, further complicated by their mechanical properties. Consequently, increasing both the measurement speed and experimental mass resolving power of these devices remains challenging. Additional improvements in data analysis and monitoring of more modes are necessary to address these issues. Cavity optomechanical systems, which enhance both mechanical and optical resonances through interactions between light and mechanical resonators, might offer a better platform through single-mode operation for precision sensing. Mass photometry is an emerging optical technique with a high dynamic mass range, needing only nanomolar concentrations of analyte, and has been used generally for examining biomolecules such as proteins. Earlier, an iSCAT technique has been employed in materials science to accurately infer the size distribution of nanoparticles by various sizes without probing their masses. Thus, MP can be used to study solution-phase polymerization, host-guest interactions, and self-assembly, similar to its use in biomolecular interactions. Also, when dispersion and heterogeneity in nanomaterial composition increase, more relevant metrics (than mass accuracy and mass resolution) are average mass and mass distribution. Clearly, dimensional nanometrology (size measurement), a pillar of nanoscience and technology must be completed by such new metrics.

While the technologies for single particle mass analysis were demonstrated some time ago, it is only in the last decade that tremendous advances have propelled the field forward. As we begin to get a glimpse of what lies ahead, there is undoubtedly a lot to learn at the interface between the molecular and the nano world.

References

1. J. R. Yates Iii, *Nature Methods*, 2011, **8**, 633-637.
2. J. H. Beynon, *Nature*, 1954, **174**, 735-737.
3. G. Siuzdak, *Proc Natl Acad Sci U S A*, 1994, **91**, 11290-11297.
4. A. C. Leney and A. J. R. Heck, *Journal of the American Society for Mass Spectrometry*, 2017, **28**, 5-13.
5. D. Z. Keifer, E. E. Pierson and M. F. Jarrold, *Analyst*, 2017, **142**, 1654-1671.
6. E. Deslignière, A. Rolland, E. H. T. M. Ebberink, V. Yin and A. J. R. Heck, *Accounts of Chemical Research*, 2023, **56**, 1458-1468.
7. C. H. Arnaud, *C&EN Global Enterprise*, 2023, **101**, 21-25.
8. S. Schmid, L. G. Villanueva and M. L. Roukes, *Fundamentals of Nanomechanical Resonators*, Springer Cham, 2016.
9. D. Cole, G. Young, A. Weigel, A. Sebesta and P. Kukura, *ACS Photonics*, 2017, **4**, 211-216.
10. M. F. Jarrold, *Chemical Reviews*, 2022, **122**, 7415-7441.
11. K. L. Brown and G. W. Tautfest, *Review of Scientific Instruments*, 1956, **27**, 696-702.
12. C. E. Sosolik, A. C. Lavery, E. B. Dahl and B. H. Cooper, *Review of Scientific Instruments*, 2000, **71**, 3326-3330.
13. U. Bahr, U. Röhling, C. Lautz, K. Strupat, M. Schürenberg and F. Hillenkamp, *International Journal of Mass Spectrometry and Ion Processes*, 1996, **153**, 9-21.
14. W. P. Peng, Y. Cai, Y. T. Lee and H. C. Chang, *International Journal of Mass Spectrometry*, 2003, **229**, 67-76.
15. W. Shockley, *Journal of Applied Physics*, 1938, **9**, 635-636.
16. H. Shelton, C. D. Hendricks, Jr. and R. F. Wuerker, *Journal of Applied Physics*, 1960, **31**, 1243-1246.
17. C. D. Hendricks, *Journal of Colloid Science*, 1962, **17**, 249-259.
18. P. W. Keaton, G. C. Idzorek, L. J. Rowton, J. D. Seagrave, G. L. Stradling, S. D. Bergeson, M. T. Collopy, H. L. Curling, D. B. McColl and J. D. Smith, *International Journal of Impact Engineering*, 1990, **10**, 295-308.
19. G. L. Stradling, G. C. Idzorek, B. P. Shafer, H. L. Curling, M. T. Collopy, A. A. H. Blossom and S. Fuerstenau, *International Journal of Impact Engineering*, 1993, **14**, 719-727.
20. R. Chen, X. Cheng, D. W. Mitchell, S. A. Hofstadler, Q. Wu, A. L. Rockwood, M. G. Sherman and R. D. Smith, *Analytical Chemistry*, 1995, **67**, 1159-1163.
21. A. Makarov, *Analytical Chemistry*, 2000, **72**, 1156-1162.
22. P. Räcke, D. Spemann, J. W. Gerlach, B. Rauschenbach and J. Meijer, *Scientific Reports*, 2018, **8**, 9781.
23. R. Antoine, *Rapid Communications in Mass Spectrometry*, 2020, **34**, e8539.
24. Z. Nie, F. Cui, Y.-K. Tzeng, H.-C. Chang, M. Chu, H.-C. Lin, C.-H. Chen, H.-H. Lin and A. L. Yu, *Analytical Chemistry*, 2007, **79**, 7401-7407.
25. H.-C. Chang, *Annual Review of Analytical Chemistry*, 2009, **2**, 169-185.
26. Y. Cai, W. P. Peng, S. J. Kuo, Y. T. Lee and H. C. Chang, *Analytical Chemistry*, 2002, **74**, 232-238.

27. W. P. Peng, H. C. Lin, H. H. Lin, M. Chu, L. Y. Alice, H. C. Chang and C. H. Chen, *Angewandte Chemie-International Edition*, 2007, **46**, 3865-3869.
28. A. Ozdemir, J.-L. Lin, M. Gulfen, S.-H. Lai, C.-J. Hsiao, N. G. Chen and C.-H. Chen, *Analytical Chemistry*, 2017, **89**, 13195-13202.
29. A. Özdemir, J.-L. Lin, M. Gülfen, C.-J. Hsiao and C.-H. Chen, *Analyst*, 2019, **144**, 5608-5616.
30. S.-Y. Liang, A. A. Patil, C.-H. Han, S.-W. Chou, W. Chang, P.-C. Soo, H.-C. Chang and W.-P. Peng, *Analytical Chemistry*, 2018, **90**, 13236-13242.
31. N. Zhang, K. Zhu, C. Xiong, Y. Jiang, H.-C. Chang and Z. Nie, *Analytical Chemistry*, 2016, **88**, 5958-5962.
32. C. Xiong, H. Liu, C. Liu, J. Xue, L. Zhan and Z. Nie, *Analytical Chemistry*, 2019, **91**, 13508-13513.
33. C. Xiong, H. Liu, Y. Li, L. Meng, J. Wang and Z. Nie, *Analytical Chemistry*, 2022, **94**, 2686-2692.
34. S. D. Fuerstenau and W. H. Benner, *Rapid Communications in Mass Spectrometry*, 1995, **9**, 1528-1538.
35. M. Gamero-Castaño, *Review of Scientific Instruments*, 2007, **78**.
36. S. H. Lai, S. Tamara and A. J. R. Heck, *iScience*, 2021, **24**, 103211.
37. https://cordis.europa.eu/project/id/964553/reporting.
38. B. Bothner and G. Siuzdak, *ChemBioChem*, 2004, **5**, 258-260.
39. M. F. Jarrold, *Journal of the American Chemical Society*, 2024, **146**, 5749-5758.
40. G. R. D. Prabhu, E. R. Williams, M. Wilm and P. L. Urban, *Nature Reviews Methods Primers*, 2023, **3**, 23.
41. B. L. Barney, R. T. Daly and D. E. Austin, *Review of Scientific Instruments*, 2013, **84**.
42. D. Hrabovsky, B. Argence, D. Lesage, P. Colomby, M. Surugue and R. B. Cole, *Analytical Chemistry*, 2024, **96**, 6986-6994.
43. J. W. Smith, E. E. Siegel, J. T. Maze and M. F. Jarrold, *Analytical Chemistry*, 2011, **83**, 950-956.
44. A. G. Elliott, S. I. Merenbloom, S. Chakrabarty and E. R. Williams, *Int J Mass Spectrom*, 2017, **414**, 45-55.
45. N. C. Contino and M. F. Jarrold, *International Journal of Mass Spectrometry*, 2013, **345-347**, 153-159.
46. N. C. Contino, E. E. Pierson, D. Z. Keifer and M. F. Jarrold, *Journal of The American Society for Mass Spectrometry*, 2013, **24**, 101-108.
47. E. E. Pierson, N. C. Contino, D. Z. Keifer and M. F. Jarrold, *Journal of the American Society for Mass Spectrometry*, 2015, **26**, 1213-1220.
48. D. Z. Keifer, D. L. Shinholt and M. F. Jarrold, *Analytical Chemistry*, 2015, **87**, 10330-10337.
49. C. C. Harper, A. G. Elliott, H.-W. Lin and E. R. Williams, *Journal of The American Society for Mass Spectrometry*, 2018, **29**, 1861-1869.
50. A. R. Todd, A. W. Alexander and M. F. Jarrold, *Journal of the American Society for Mass Spectrometry*, 2020, **31**, 146-154.
51. A. R. Todd and M. F. Jarrold, *Journal of the American Society for Mass Spectrometry*, 2020, **31**, 1241-1248.
52. A. R. Todd, L. F. Barnes, K. Young, A. Zlotnick and M. F. Jarrold, *Analytical Chemistry*, 2020, **92**, 11357-11364.
53. D. Y. Botamanenko, D. W. Reitenbach, L. M. Miller and M. F. Jarrold, *Journal of the American Society for Mass Spectrometry*, 2023, **34**, 1731-1740.
54. A. G. Elliott, C. C. Harper, H.-W. Lin and E. R. Williams, *Analyst*, 2017, **142**, 2760-2769.
55. C. C. Harper and E. R. Williams, *Journal of the American Society for Mass Spectrometry*, 2019, **30**, 2637-2645.
56. R. A. Zubarev and A. Makarov, *Analytical Chemistry*, 2013, **85**, 5288-5296.
57. J. E. Bruce, G. A. Anderson, H. R. Udseth and R. D. Smith, *Analytical Chemistry*, 1998, **70**, 519-525.

58. A. Makarov and E. Denisov, *Journal of the American Society for Mass Spectrometry*, 2009, **20**, 1486-1495.
59. J. O. Kafader, R. D. Melani, M. W. Senko, A. A. Makarov, N. L. Kelleher and P. D. Compton, *Analytical Chemistry*, 2019, **91**, 2776-2783.
60. R. D. Smith, *Journal of the American Society for Mass Spectrometry*, 2023, **34**, 803-812.
61. J. O. Kafader, R. D. Melani, K. R. Durbin, B. Ikwuagwu, B. P. Early, R. T. Fellers, S. C. Beu, V. Zabrouskov, A. A. Makarov, J. T. Maze, D. L. Shinholt, P. F. Yip, D. Tullman-Ercek, M. W. Senko, P. D. Compton and N. L. Kelleher, *Nature Methods*, 2020, **17**, 391-394.
62. T. P. Wörner, J. Snijder, A. Bennett, M. Agbandje-McKenna, A. A. Makarov and A. J. R. Heck, *Nature Methods*, 2020, **17**, 395-398.
63. J. W. Hoyes, G., presented in part at the American Society for Mass Spectrometry, Philadelphia, 2021.
64. J. O. Kafader, S. C. Beu, B. P. Early, R. D. Melani, K. R. Durbin, V. Zabrouskov, A. A. Makarov, J. T. Maze, D. L. Shinholt, P. F. Yip, N. L. Kelleher, P. D. Compton and M. W. Senko, *Journal of The American Society for Mass Spectrometry*, 2019, **30**, 2200-2203.
65. M. M. Kostelic, C. K. Zak, Y. Liu, V. S. Chen, Z. Wu, J. Sivinski, E. Chapman and M. T. Marty, *Analytical Chemistry*, 2021, **93**, 14722-14729.
66. T. Doussineau, M. Kerleroux, X. Dagany, C. Clavier, M. Barbaire, J. Maurelli, R. Antoine and P. Dugourd, *Rapid Communications in Mass Spectrometry*, 2011, **25**, 617-623.
67. J. T. Maze, T. C. Jones and M. F. Jarrold, *The Journal of Physical Chemistry A*, 2006, **110**, 12607-12612.
68. C. C. Harper, D. D. Brauer, M. B. Francis and E. R. Williams, *Chemical Science*, 2021, **12**, 5185-5195.
69. J. C. Schultz, C. A. Hack and W. H. Benner, *Journal of the American Society for Mass Spectrometry*, 1998, **9**, 305-313.
70. M. A. Halim, F. Bertorelle, T. Doussineau and R. Antoine, *Rapid Communications in Mass Spectrometry*, 2019, **33**, 35-39.
71. T. Doussineau, R. Antoine, M. Santacreu and P. Dugourd, *The Journal of Physical Chemistry Letters*, 2012, **3**, 2141-2145.
72. T. Doussineau, A. Désert, O. Lambert, J.-C. Taveau, M. Lansalot, P. Dugourd, E. Bourgeat-Lami, S. Ravaine, E. Duguet and R. Antoine, *The Journal of Physical Chemistry C*, 2015, **119**, 10844-10849.
73. C. C. Harper, Z. M. Miller, M. S. McPartlan, J. S. Jordan, R. E. Pedder and E. R. Williams, *ACS Nano*, 2023, **17**, 7765-7774.
74. L. M. Miller, T. W. Young, Y. Wang, B. E. Draper, X. Ye, S. C. Jacobson and M. F. Jarrold, *Analytical Chemistry*, 2024, **96**, 14239-14247.
75. D. Bain, I. Russier-Antoine, H. Yuan, S. Kolay, S. Maclot, C. Moulin, E. Salmon, P.-F. Brevet, A. Pniakowska, J. Olesiak-Bańska and R. Antoine, *Langmuir*, 2023, **39**, 16554-16561.
76. S. Basu, H. Fakhouri, C. Moulin, S. Dolai, I. Russier-Antoine, P.-F. Brevet, R. Antoine and A. Paul, *Nanoscale*, 2021, **13**, 4439-4443.
77. A. Tsirkou, F. Kaczorowski, M. Verdurand, R. Raffoul, J. Pansieri, I. Quadrio, F. Chauveau and R. Antoine, *Chemical Communications*, 2022, **58**, 7192-7195.
78. T. Doussineau, C. Mathevon, L. Altamura, C. Vendrely, P. Dugourd, V. Forge and R. Antoine, *Angewandte Chemie International Edition*, 2016, **55**, 2340-2344.
79. J. Pansieri, M. A. Halim, C. Vendrely, M. Dumoulin, F. Legrand, M. M. Sallanon, S. Chierici, S. Denti, X. Dagany and P. Dugourd, *Chemical Science*, 2018, **9**, 2791-2796.
80. B. A. Brown, X. Zeng, A. R. Todd, L. F. Barnes, J. M. A. Winstone, J. C. Trinidad, M. V. Novotny, M. F. Jarrold and D. E. Clemmer, *Analytical Chemistry*, 2020, **92**, 3285-3292.
81. L. M. Miller and M. F. Jarrold, *Essays Biochem*, 2023, **67**, 315-323.

82. M. A. den Boer, S.-H. Lai, X. Xue, M. D. van Kampen, B. Bleijlevens and A. J. R. Heck, *Analytical Chemistry*, 2022, **94**, 892-900.
83. K. G. Andersen, A. Rambaut, W. I. Lipkin, E. C. Holmes and R. F. Garry, *Nature Medicine*, 2020, **26**, 450-452.
84. L. M. Miller, L. F. Barnes, S. A. Raab, B. E. Draper, T. J. El-Baba, C. A. Lutomski, C. V. Robinson, D. E. Clemmer and M. F. Jarrold, *Journal of the American Chemical Society*, 2021, **143**, 3959-3966.
85. V. Yin, S. H. Lai, T. G. Caniels, P. J. M. Brouwer, M. Brinkkemper, Y. Aldon, H. Liu, M. Yuan, I. A. Wilson, R. W. Sanders, M. J. van Gils and A. J. R. Heck, *ACS Cent Sci*, 2021, **7**, 1863-1873.
86. N. R. Genuth and M. Barna, *Molecular Cell*, 2018, **71**, 364-374.
87. T. P. Wörner, A. Bennett, S. Habka, J. Snijder, O. Friese, T. Powers, M. Agbandje-McKenna and A. J. R. Heck, *Nature Communications*, 2021, **12**, 1642.
88. L. F. Barnes, B. E. Draper, Y.-T. Chen, T. W. Powers and M. F. Jarrold, *Molecular Therapy Methods & Clinical Development*, 2021, **23**, 87-97.
89. T. P. Wörner, J. Snijder, O. Friese, T. Powers and A. J. R. Heck, *Molecular Therapy Methods & Clinical Development*, 2022, **24**, 40-47.
90. E. H. T. M. Ebberink, A. Ruisinger, M. Nuebel, M. Thomann and A. J. R. Heck, *Molecular Therapy Methods & Clinical Development*, 2022, **27**, 491-501.
91. L. M. Miller, K. M. Bond, B. E. Draper and M. F. Jarrold, *Analytical Chemistry*, 2021, **93**, 11965-11972.
92. A. C. Susa, Z. Xia and E. R. Williams, *Angewandte Chemie International Edition*, 2017, **56**, 7912-7915.
93. Z. M. Miller, C. C. Harper, H. Lee, A. J. Bischoff, M. B. Francis, D. V. Schaffer and E. R. Williams, *Journal of the American Society for Mass Spectrometry*, 2022, **33**, 2129-2137.
94. W. P. Poschenrieder, *International Journal of Mass Spectrometry and Ion Physics*, 1972, **9**, 357-373.
95. H. D. P. A. L. Y. T. A. K. I. Filippov, presented in part at the American Society for Mass Spectrometry, Houston, 2023.
96. H. T. Schmidt, H. Cederquist, J. Jensen and A. Fardi, *Nuclear Instruments and Methods in Physics Research Section B: Beam Interactions with Materials and Atoms*, 2001, **173**, 523-527.
97. W. H. Benner, *Analytical Chemistry*, 1997, **69**, 4162-4168.
98. T. P. Wörner, K. Aizikov, J. Snijder, K. L. Fort, A. A. Makarov and A. J. R. Heck, *Nature Chemistry*, 2022, **14**, 515-522.
99. Y. Lyutvinskiy, K. O. Nagornov, A. N. Kozhinov, N. Gasilova, L. Menin, Z. Meng, X. Zhang, A. A. Saei, T. Fu, J. Chamot-Rooke, Y. O. Tsybin, A. Makarov and R. A. Zubarev, *Journal of the American Society for Mass Spectrometry*, 2024, **35**, 902-911.
100. J. O. Kafader, K. R. Durbin, R. D. Melani, B. J. Des Soye, L. F. Schachner, M. W. Senko, P. D. Compton and N. L. Kelleher, *Journal of Proteome Research*, 2020, **19**, 1346-1350.
101. J. P. Cleveland, S. Manne, D. Bocek and P. K. Hansma, *Review of Scientific Instruments*, 1993, **64**, 403-405.
102. T. Thundat, E. A. Wachter, S. L. Sharp and R. J. Warmack, *Applied Physics Letters*, 1995, **66**, 1695-1697.
103. Y. T. Yang, K. L. Ekinci, X. M. H. Huang, L. M. Schiavone, M. L. Roukes, C. A. Zorman and M. Mehregany, *Applied Physics Letters*, 2001, **78**, 162-164.
104. P. Mohanty, D. A. Harrington, K. L. Ekinci, Y. T. Yang, M. J. Murphy and M. L. Roukes, *Physical Review B*, 2002, **66**, 085416.
105. K. L. Ekinci, Y. T. Yang, X. M. H. Huang and M. L. Roukes, *Applied Physics Letters*, 2002, **81**, 2253-2255.
106. K. L. Ekinci, Y. T. Yang and M. L. Roukes, *Journal of Applied Physics*, 2004, **95**, 2682-2689.
107. K. L. Ekinci, X. M. H. Huang and M. L. Roukes, *Applied Physics Letters*, 2004, **84**, 4469-4471.

108. M. Li, H. X. Tang and M. L. Roukes, *Nature Nanotechnology*, 2007, **2**, 114-120.
109. E. Mile, G. Jourdan, I. Bargatin, S. Labarthe, C. Marcoux, P. Andreucci, S. Hentz, C. Kharrat, E. Colinet and L. Duraffourg, *Nanotechnology*, 2010, **21**, 165504.
110. M. Sansa, E. Sage, E. C. Bullard, M. Gély, T. Alava, E. Colinet, A. K. Naik, L. G. Villanueva, L. Duraffourg, M. L. Roukes, G. Jourdan and S. Hentz, *Nature Nanotechnology*, 2016, **11**, 552-558.
111. J. Chaste, A. Eichler, J. Moser, G. Ceballos, R. Rurali and A. Bachtold, *Nature Nanotechnology*, 2012, **7**, 301-304.
112. I. Bargatin, I. Kozinsky and M. L. Roukes, *Applied Physics Letters*, 2007, **90**.
113. M. S. Hanay, S. Kelber, A. K. Naik, D. Chi, S. Hentz, E. C. Bullard, E. Colinet, L. Duraffourg and M. L. Roukes, *Nature Nanotechnology*, 2012, **7**, 602-608.
114. A. Demir, *IEEE Sensors Journal*, 2021, **21**, 27582-27589.
115. T. Fortin, B. Vysotskyi, M. Defoort, A. Reynaud, S. H. Lai, S. Dominguez-Medina, K. Clement, V. Cumaku, S. Hentz and C. Masselon, *IEEE Sensors Journal*, 2021, **21**, 21852-21861.
116. A. P. Neumann, A. Gomez, A. R. Nunn, J. E. Sader and M. L. Roukes, *Review of Scientific Instruments*, 2024, **95**.
117. O. Malvar, J. J. Ruz, P. M. Kosaka, C. M. Domínguez, E. Gil-Santos, M. Calleja and J. Tamayo, *Nature Communications*, 2016, **7**, 13452.
118. S. Dominguez-Medina, S. Fostner, M. Defoort, M. Sansa, A. K. Stark, M. A. Halim, E. Vernhes, M. Gely, G. Jourdan, T. Alava, P. Boulanger, C. Masselon and S. Hentz, *Science*, 2018, **362**, 918-922.
119. M. Sansa, M. Defoort, A. Brenac, M. Hermouet, L. Banniard, A. Fafin, M. Gely, C. Masselon, I. Favero, G. Jourdan and S. Hentz, *Nature Communications*, 2020, **11**, 3781.
120. E. Sage, M. Sansa, S. Fostner, M. Defoort, M. Gély, A. K. Naik, R. Morel, L. Duraffourg, M. L. Roukes, T. Alava, G. Jourdan, E. Colinet, C. Masselon, A. Brenac and S. Hentz, *Nature Communications*, 2018, **9**, 3283.
121. R. T. Erdogan, M. Alkhaled, B. E. Kaynak, H. Alhmoud, H. S. Pisheh, M. Kelleci, I. Karakurt, C. Yanik, Z. B. Şen, B. Sari, A. M. Yagci, A. Özkul and M. S. Hanay, *ACS Nano*, 2022, **16**, 3821-3833.
122. M. S. Hanay, S. I. Kelber, C. D. O'Connell, P. Mulvaney, J. E. Sader and M. L. Roukes, *Nature Nanotechnology*, 2015, **10**, 339-344.
123. A. K. Naik, M. S. Hanay, W. K. Hiebert, X. L. Feng and M. L. Roukes, *Nature Nanotechnology*, 2009, **4**, 445-450.
124. E. Sage, A. Brenac, T. Alava, R. Morel, C. Dupré, M. S. Hanay, M. L. Roukes, L. Duraffourg, C. Masselon and S. Hentz, *Nature Communications*, 2015, **6**, 6482.
125. E. Sage, O. Martin, C. Dupré, T. Ernst, G. Billiot, L. Duraffourg, E. Colinet and S. Hentz, 2013.
126. US 9,506,852 B2, 2016.
127. B. E. Kaynak, M. Alkhaled, E. Kartal, C. Yanik and M. S. Hanay, *Nano Letters*, 2023, **23**, 8553-8559.
128. B.-B. Li, L. Ou, Y. Lei and Y.-C. Liu, *Nanophotonics*, 2021, **10**, 2799-2832.
129. M. Hermouet, M. Sansa, M. Defoort, L. Banniard, S. Dominauez-Medina, S. Fostner, U. Palanchoke, A. Fafin, M. Gely, L. Hutin, P. Christophe, E. Rolland, C. Tabone, G. Usai, T. Ernst, P. Villard, G. Billiot, P. Mattei, G. Nonglaton and S. Hentz, *Very Large Scale Integration Optomechanics: a cure for loneliness of NEMS resonators?*, 2018.
130. K. Clement, A. Reynaud, M. Defoort, B. Vysotskyi, T. Fortin, S.-H. Lai, V. Çumaku, S. Dominguez-Medina, S. Hentz and C. Masselon, *Analytical and Bioanalytical Chemistry*, 2021, **413**, 7147-7156.
131. S.-H. Lai, A. Reynaud, N.-N. Zhang, M. Kwak, B. Vysotskyi, S. Dominguez-Medina, T. Fortin, K. Clement, M. Defoort, T. G. Lee, K. Liu, S. Hentz and C. D. Masselon, *The Journal of Physical Chemistry C*, 2022, **126**, 20946-20953.
132. L. Priest, J. S. Peters and P. Kukura, *Chemical Reviews*, 2021, **121**, 11937-11970.
133. J. O. Arroyo and P. Kukura, *Nature Photonics*, 2016, **10**, 11-17.
134. R. W. Taylor and V. Sandoghdar, *Nano Letters*, 2019, **19**, 4827-4835.

135. G. Young and P. Kukura, *Annual Review of Physical Chemistry*, 2019, **70**, 301-322.
136. Y.-F. Huang, G.-Y. Zhuo, C.-Y. Chou, C.-H. Lin, W. Chang and C.-L. Hsieh, *ACS Nano*, 2017, **11**, 2575-2585.
137. M. Liebel, J. T. Hugall and N. F. van Hulst, *Nano Letters*, 2017, **17**, 1277-1281.
138. G. Young, N. Hundt, D. Cole, A. Fineberg, J. Andrecka, A. Tyler, A. Olerinyova, A. Ansari, E. G. Marklund, M. P. Collier, S. A. Chandler, O. Tkachenko, J. Allen, M. Crispin, N. Billington, Y. Takagi, J. R. Sellers, C. Eichmann, P. Selenko, L. Frey, R. Riek, M. R. Galpin, W. B. Struwe, J. L. P. Benesch and P. Kukura, *Science*, 2018, **360**, 423-427.
139. F. Soltermann, E. D. B. Foley, V. Pagnoni, M. Galpin, J. L. P. Benesch, P. Kukura and W. B. Struwe, *Angewandte Chemie International Edition*, 2020, **59**, 10774-10779.
140. Y. Tomioka, R. Sato, R. Takahashi, S. Nagatoishi, K. Shiba, K. Tsumoto, T. Arakawa and T. Akuta, *Biophysical Chemistry*, 2023, **296**, 106977.
141. X. Huang, H. Kamadurai, P. Siuti, E. Ahmed, J. L. Bennett and W. A. Donald, *Journal of the American Chemical Society*, 2023, **145**, 14716-14726.
142. D. Wu and G. Piszczek, *Analytical Biochemistry*, 2020, **592**, 113575.
143. H. Gizardin-Fredon, P. E. Santo, M.-E. Chagot, B. Charpentier, T. M. Bandeiras, X. Manival, O. Hernandez-Alba and S. Cianférani, *Nature Communications*, 2024, **15**, 3516.
144. Y. Li, W. B. Struwe and P. Kukura, *Nucleic Acids Research*, 2020, **48**, e97-e97.
145. R. F. Garmann, A. M. Goldfain, C. R. Tanimoto, C. E. Beren, F. F. Vasquez, D. A. Villarreal, C. M. Knobler, W. M. Gelbart and V. N. Manoharan, *Proceedings of the National Academy of Sciences*, 2022, **119**, e2206292119.
146. D. A. T. Cramer, V. Franc, A.-K. Heidenreich, M. Hook, M. Adibzadeh, D. Reusch, A. J. R. Heck and M. Haberger, *mAbs*, 2023, **15**, 2175312.
147. D. Wu, P. Hwang, T. Li and G. Piszczek, *Gene Therapy*, 2022, **29**, 691-697.
148. L. Melo, A. Hui, M. Kowal, E. Boateng, Z. Poursorkh, E. Rocheron, J. Wong, A. Christy and E. Grant, *The Journal of Physical Chemistry B*, 2021, **125**, 12466-12475.
149. J. Roy, I. Marathe, V. H. Wysocki and T. Pradeep, *Chemical Communications*, 2024, DOI: 10.1039/D4CC00363B.
150. A. Sonn-Segev, K. Belacic, T. Bodrug, G. Young, R. T. VanderLinden, B. A. Schulman, J. Schimpf, T. Friedrich, P. V. Dip, T. U. Schwartz, B. Bauer, J.-M. Peters, W. B. Struwe, J. L. P. Benesch, N. G. Brown, D. Haselbach and P. Kukura, *Nature Communications*, 2020, **11**, 1772.
151. S. S. Paul, A. Lyons, R. Kirchner and M. T. Woodside, *ACS Nano*, 2022, **16**, 16462-16470.
152. E. D. B. Foley, M. S. Kushwah, G. Young and P. Kukura, *Nature Methods*, 2021, **18**, 1247-1252.
153. T. Heermann, F. Steiert, B. Ramm, N. Hundt and P. Schwille, *Nature Methods*, 2021, **18**, 1239-1246.
154. C. Hiemenz, N. Baumeister, C. Helbig, A. Hawe, S. Babutzka, S. Michalakis, W. Friess and T. Menzen, *Molecular Therapy - Methods & Clinical Development*, 2023, **31**, 101162.
155. E. H. T. M. Ebberink, A. Ruisinger, M. Nuebel, H. Meyer-Berg, I. R. S. Ferreira, M. Thomann and A. J. R. Heck, *Molecular Therapy Methods & Clinical Development*, 2024, **32**.
156. R. A. Parikh, B. E. Draper and M. F. Jarrold, *Analytical Chemistry*, 2024, **96**, 3062-3069.